Chapter 4

Interference Cancellation in HSDPA Terminals

Ahmet Başтuğ, Irfan Ghauri, and Dirk T.M. Slock

Contents

4.1 Introduction

Over-the-air communication is interference limited. Deployment of wireless networks therefore needs resource planning. Neighboring base stations in a cellular network could, for instance, transmit in different frequency bands. For such deployment, hexagonal cell geometry is assumed in cellular systems (see Figure 4.1), and resource planning is done by allocation of disjoint chunks of spectrum to neighboring base stations. The number of neighboring cells in which a certain frequency can be used only once is known in the cellular literature as the *frequency reuse factor*. A frequency reuse factor of 7 results when isotropic antennas are deployed at cell-site (base station) and of 3 when using antenna sectorization of three sectors per hexagonal cell. Such frequency planning obviously aims interference avoidance, but it makes network deployment cumbersome and is wasteful of spectral resources. A direct sequence (DS)-CDMA (Code Division Multiple Access) system, in principle, boasts a frequency reuse factor of 1. In fact, this factor was purportedly one of the main advantages of the first CDMA-based cellular network, IS-95 [41]. Users can coexist in the same frequency spectrum. A resource is a spreading code and in the specific case of downlink communications, codes belong to a binary orthogonal set, the Walsh-Hadamard set. A base station has the entire set of codes at its disposal.

All base stations employ the same code-set as resources, and each base station overlays a frame containing a number of spread symbols by a specific long pseudo-random code with quarternary alphabet called the scrambling code. The code helps the mobile station distinguish between base station signals.

Standard CDMA mobile receivers are matched filters, matched to the spreading code of the signal (user) of which one needs to detect transmitted symbols. When the signal passes through a multipath channel, the receiver is matched to the cascade of the spreading code and the channel. The matched filter is also called a RAKE receiver in the context of multipath signal due to one standard correlator-based implementation that resembles an agricultural rake. In this receiver energy in delayed multipath signals is collected by correlating the delayed copies of the signal with the code of the user of interest.

User-specific spreading and base station–specific scrambling are the key elements of the general structure of downlink communications in early-day CDMA systems such as IS-95 and even circuit-switched UMTS (Universal Mobile Telecommunication System) [4], both of which support low-rate applications. In the latter, maximum service data rates of 384 kbps per base station using all physical channels resources are achievable. Such rates are sufficient for applications such as video streaming.

Spreading and scrambling at the transmitter and corresponding descrambling and despreading at the receiver do not fundamentally change the communication paradigm but are simply elements of the multiple access method (CDMA). It is hoped that noise-like user signals rendered thus due to bandwidth expansion (spreading) will be rejected by the matched filter. All other transceiver stages, such as error-control coding and interleaving to mitigate block-fading, are similar to those in single-user communications.

A mobile station can be affected by two types of interference known in the literature as intra-cell and inter-cell interference. In the particular case of downlink CDMA communications, which we shall henceforth address, the former comes about due to multipath propagation in the channel. Indeed, the channel distorts signals in transit that were orthogonal upon transmission. The RAKE receiver is then limited in performance due to this interference, sometimes also referred to as self-interference because even in the case of one trasmitted code, copies of the signal interfere mutually. This is no different from the inter-symbol-interference (ISI) problem in band-limited channels. It is shown in [38] that the signal-to-interference-plus-noise ratio (SINR) of the RAKE receiver contains a per-code interference term that is the sum of energies of all multipath components at the RAKE output scaled by the inverse of the spreading factor. As the number of codes increases for a given spreading factor (SF), as is the case in High-Speed Downlink Packet Access (HSDPA) where up to 15 codes with SF 16 can co-exist, the SINR at the RAKE output may degrade sufficiently to render communication unreliable. Mitigation of intra-cell interference can be done through equalization prior to despreading receivers [13].

In the downlink (HSDPA) context, inter-cell interference is the signal a mobile station sees from one or more neighboring base stations. Due to propagation factors, the cell boundary is not really a regular contour (e.g., a hexagon) and is only of figurative interest. When frequency reuse is unity, a good way of delimiting a cell is the strength of the signal. However, with full frequency reuse as in the case in CDMA, the signal-to-interference ratio (SIR) experienced at the mobile station is a more appropriate cell boundary notion. Users experience increasing levels of interference as they move from the base station/cell site toward the cell boundary. As interference could be a sum of interferences from several neighboring cell sites, it is customary [5] to define SIR as the signal to total-intercell-interferences ratio, and each interfering station to total inter-cell interference ratio is referred to

as the dominant interference portion (DIP) ratio. Some reference numbers for these quantities are SIR of 0 dB with two interfering base stations with DIP of −2.75 and −7.64 dB respectively [5].

This chapter is organized as follows. The section entitled "UMTS Downlink and HSDPA" revisits the UMTS downlink signal and discusses HSDPA in relation with early-day non-packet UMTS. The section entitled "Downlink Channel and HSDPA Signal Models" describes the propagation environment and the channel model. The section entitled "Suppression of Intra-cell Interference in HSDPA" addresses the RAKE receiver, and some linear chip-level equalizers capable of dealing with intra-cell interference. The section entitled "Advanced Receivers for Interference Cancellation" discusses inter-cell interference and presents a variety of solutions for suppression of this interference.

4.2 UMTS Downlink and HSDPA

We limit ourselves to the discussion of the UMTS WCDMA standard, of which HSDPA is one component. This system is based on frequency division duplexing (FDD) so that uplink and downlink transmissions occur in non-overlapping frequency bands. Thus, a mobile terminal sees only signals from base stations. Another version of UMTS uses time division duplexing (TDD) where mobile terminals could effectively see interference from terminals talking to other base stations unless strict time-scheduling rules are introduced. Despite being an interesting problem itself, UMTS TDD is beyond the scope of this discussion.

4.2.1 Multiple Access in UMTS FDD Downlink

In the UMTS downlink, base stations transmit in frequency bands of 5 MHz around the 2.1-GHz frequency. Each UMTS operator in general has two or three bands for downlink transmission. The base station, which is known as Node B in the UMTS radio access network (RAN) context, is the source of transmissions for its *logical cell*. If a sectorized cell planning is deployed, then Node B is responsible for more than one logical cell, as shown in Figure 4.1.

The signals transmitted from different logical cells are differentiated from each other by the assignment of different pseudo-random *scrambling* codes that are repeated every UMTS *frame* of 38,400 chips, and hence are known as *long* overlay codes.

Multiple access of the users in the same logical cell is realized by a CDMA scheme that uses *short* orthogonal *channelization* codes from various levels of the OVSF code tree shown in Figure 4.2. Each level of the code tree

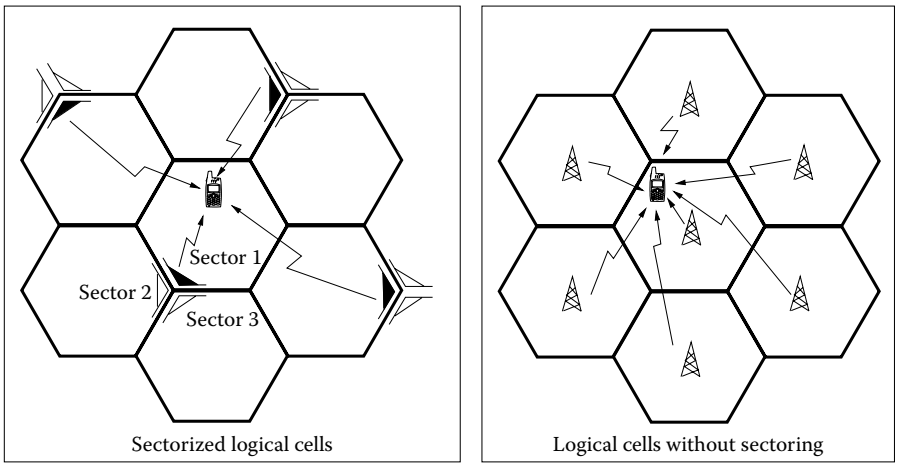

Figure 4.1 Logical cells differentiated by scrambling codes. (Also one frequency per cell in FDMA systems.)

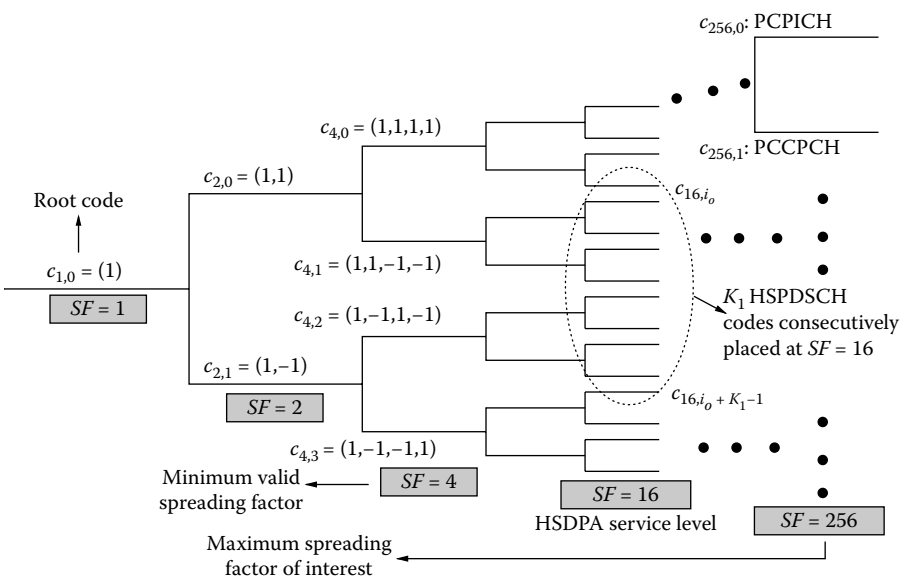

Figure 4.2 Partial schematic of the OVSF code tree.

contains codes corresponding to the columns of the Walsh-Hadamard transform (WHT) of relevant size. A channelization code assigned to a user is periodically used for the transmission of each symbol. Any particular code in the ith position at the SF level t is related to its two closest child codes at SF level $t+1$ with the transformation

$$\left[\boldsymbol{c}_{2^{t+1},2^t}\ \boldsymbol{c}_{2^{t+1},2^t+1}\right] = \begin{bmatrix} 1 & 1 \\ 1 & -1 \end{bmatrix} \otimes \boldsymbol{c}_{2^t,i} \tag{4.1}$$

where $\otimes$ stands for the Kronecker product. The valid code lengths are from the set $\{2^t,\ \ t \in 2, 3, \ldots, 9\}$. The largest code length (i.e., the spreading factor 512) is very rarely used. When a particular code is assigned to a user, then all its parent or child codes are blocked for usage in order to preserve orthogonality among the used codes. These properties make UMTS FDD downlink a *code-limited* system. In case only a single spreading level is used from the OVSF tree, then the number of available codes for that particular scenario is upper bounded by the associated spreading factor.

4.2.2 UMTS Services

The flexibility of using different length codes makes UMTS a *multi-rate* system, enabling services with different data rates and thus different quality-of-service (QoS).

Just like any other cellular multi-access system, a UMTS network must support a large number of users with different QoS and have ubiquitous coverage. Large coverage area of individual cells (i.e., decreasing the number of deployed base stations) decreases network user capacity. On the other hand, more cells would mean more inter-cell interference. From this relationship it is easy to see that in order to meet both coverage and user capacity requirements, advanced transmission (diversity) or reception techniques are of use. The UMTS standard defines four QoS classes with differing delay and packet-ordering requirements [3]:

1. *Conversational:* low delay, strict ordering (e.g., voice)
2. *Streaming:* modest delay, strict ordering (e.g., video)
3. *Interactive:* modest delay, modest ordering (e.g., web browsing)
4. *Background:* no delay guarantee, no ordering (e.g., bulk data transfer)

4.2.3 HSDPA Features

Background and *interactive* UMTS service classes have a burst nature enabling time-divided multi-user scheduling, thus reaping the benefits of

multi-user diversity [42]. This consideration triggered time-sharing system resources among users, most importantly the orthogonal codes in the downlink leading to the standardization of HSDPA in the UMTS Standard Release 5 [5].

- *Allocation of multiple access codes for HSDPA service:* Motivated by the bursty nature of the data, as shown in Figure 4.2, $K_1 \in \{1, 2, \ldots, 15\}$, of the 16 channelization code resources at SF = 16 are allocated as High-Speed Physical Downlink Shared Channels (HS-PDSCHs) these codes are dynamically time multiplexed among users in order to achieve a higher spectral efficiency and a larger link adaptation dynamic range. The variable $i_o \in \{1, 2, \ldots, 15\}$ denotes the position of the first HSPDSCH code.
- *Fast scheduling of allocated codes:* Multi-user diversity is obtained if there are independently varying temporal channel conditions for different users, leading to significantly increase in *sum capacity*, that is, the total delivered payload by the base station (BS). By one extreme approach, as demonstrated in Figure 4.3 in a simple two-user system context, one can preferably assign all the codes to a single user with the instantaneously best channel conditions, thus maximizing the throughput. At the other extreme, users might be served in a *fair* round-robin fashion. In this respect, operators are free to choose any set of schedulers compromising throughput and fairness by basing their decisions on the predicted channel quality, the cell load, and the traffic priority class. In order to reduce the delay in signaling and to better track the channel variations, scheduling is performed at Node B, which is closer to the air interface compared to the radio network controller (RNC), which was responsible for such tasks in the earlier UMTS releases. Moreover, the scheduling period decreases to 2-ms. sub-frame duration (i.e., 1 TTI, transmission time interval), from the

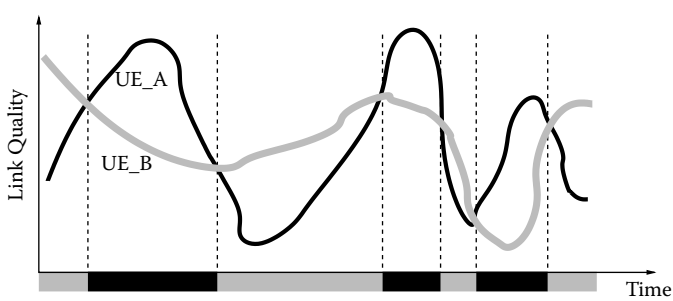

Figure 4.3 Principle of multi-user diversity.

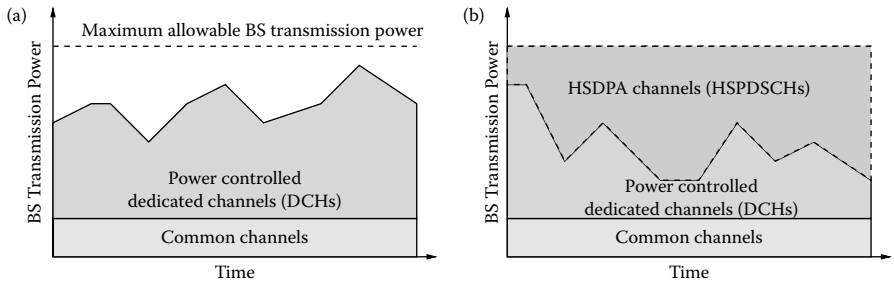

Figure 4.4 Power control with and without HSDPA. (a) UMTS FDD downlink *R99* power control mechanism, (b) UMTS FDD downlink *R5* power control mechanism.

10-ms frame duration of pre-HSDPA UMTS[1]. Soft handover is also replaced by fast *best-signaling-cell* selection, which can be considered a kind of *spatial* scheduling complementing the *temporal* scheduling.

- *Link adaptation:* As schematically demonstrated in Figure 4.4, perhaps one of the most important differences between HSDPA and its packet-switched ancestor (Release 99 or R99 UMTS) is that there is *no fast power control* on HSPDSCHs, and all the instantaneously remaining *allowed* BS power is assigned to HSPDSCHs, which creates a high amount of power variation of HSPDSCH codes [2] over time. In this case, as can be interpreted from the figure, the system is also capable of utilizing the available BS power more efficiently than the power-controlled case. Furthermore, as shown in Figure 4.9, different user distances from the BS and different user mobility levels create a high amount of *inter-user link quality* differences. These two properties make Node B scheduling more versatile in deciding the number of allocated HSPDSCH codes, coding rate, puncturing rate, and the modulation scheme. 16-QAM (quadrature amplitude modulation) a possibility in addition to QPSK (quadrature phase-shift keying) high received power conditions, to maximize the throughput of the instantaneously scheduled user. For this purpose, Node B might use either the explicit channelquality indicator (CQI) measurement reports from the UE based on the SINR of PCPICH or the known transmit power of the power-controlled downlink dedicated physical channel (DPCH) associated with the HS-PDSCHs.

[1] Low-end and medium-end HSDPA UEs (user equipments) that do not have enough buffering capability are obliged to wait at least two or three TTI periods, respectively, between two consecutive TTI data scheduling [5].

- *Hybrid Automatic Repeat reQuest (HARQ):* When transmission entities are identified to be erroneous by a standard protocol such as *selective-repeat* or *stop-and-wait*, fast retransmit request is done from Node B and combinations of soft information from the original transmission and previous retransmissions are combined to increase the probability of correct reception [19,39]. These operations compensate for errors in the channel quality estimates used for link adaptation. Two well-known methods are *chase combining*, where weighting of identical retransmissions is done, and the *incremental redundancy*, where additional parity bits are sent each retransmission.

To support the listed functionalities, two new channel types are introduced. In the downlink, one or more High-Speed Shared Control Channels (HSSCCHs) broadcast the scheduled UE identity, the transport format and the HARQ process identifier. The UE monitors up to four different HSSCCHs and tries to find out if it is going to be scheduled, or not. In the uplink, the High-Speed Dedicated Physical Control Channel (HSDPCCH) carries the status reports for HARQ and the CQIs. Figure 4.5 briefly demonstrates the order of events in the HSDPA transmission protocol. More detailed timing information and the slot structures are given in Figure 4.6, together with other UMTS channels relevant for this.

The HSSCCH is frame aligned with the PCPICH, which is generally used as a reference by several other UMTS channels and synchronization procedures as well.

HSPDSCHs are offset by two time slots with respect to HSSCCH, which gives the UE enough time to decode the time-critical control and supervision

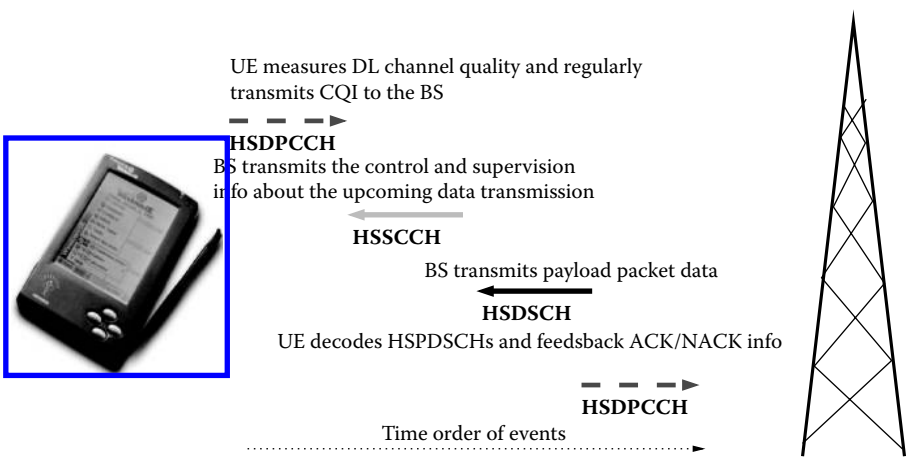

Figure 4.5 HSDPA transmission protocol.

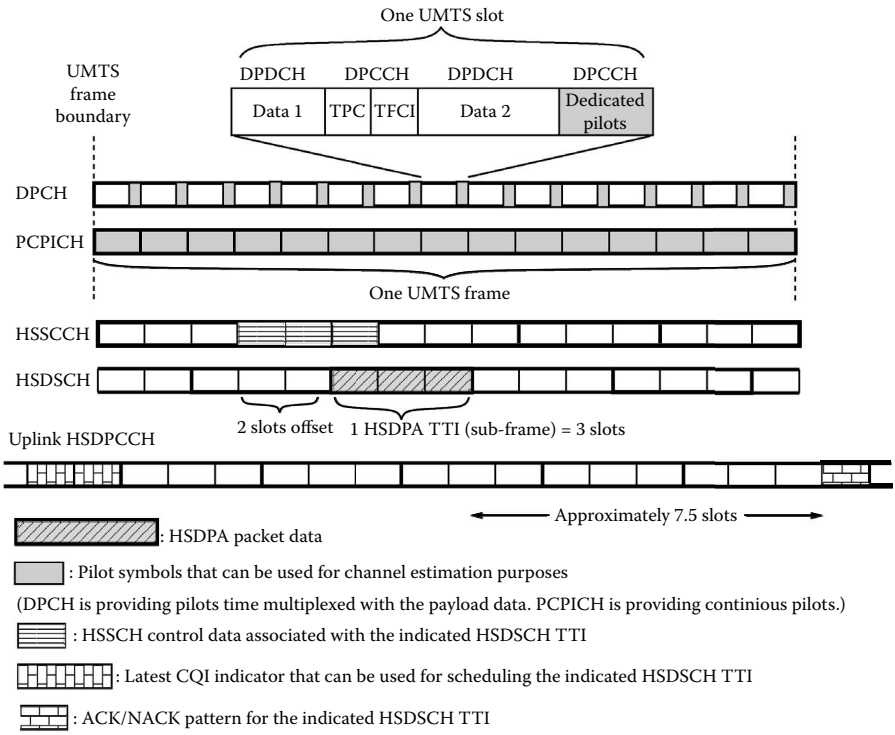

Figure 4.6 Slot structures and timings of UMTS channels of interest.

information carried by the first slot of HSSCCH before receiving the HSDSCH payload data. Learning the scheduling of UE two slots beforehand is at the same time very useful for the *adaptive* equalizers that we discuss in subsequent sections. To do power savings, it is generally preferable to freeze the adaptation mechanism of an equalizer when the UE does not receive any HSDPA data. On the other hand, it is beneficial to start the adaptation process some time earlier than the start of the data reception to enable the equalizer to converge earlier.

For detailed description of HSDPA, see [1,6,12,17].

4.2.4 Downlink Transmission Model

The baseband downlink transmission model of the UMTS-FDD mode system with HSDPA support is given in Figure 4.7.

At the transmitter, the first group of K_1 i.i.d. QPSK or 16-QAM modulated symbol sequences $\{a_1[n], a_2[n], \ldots, a_{K_1}[n]\}$, which belong to the HSDPA

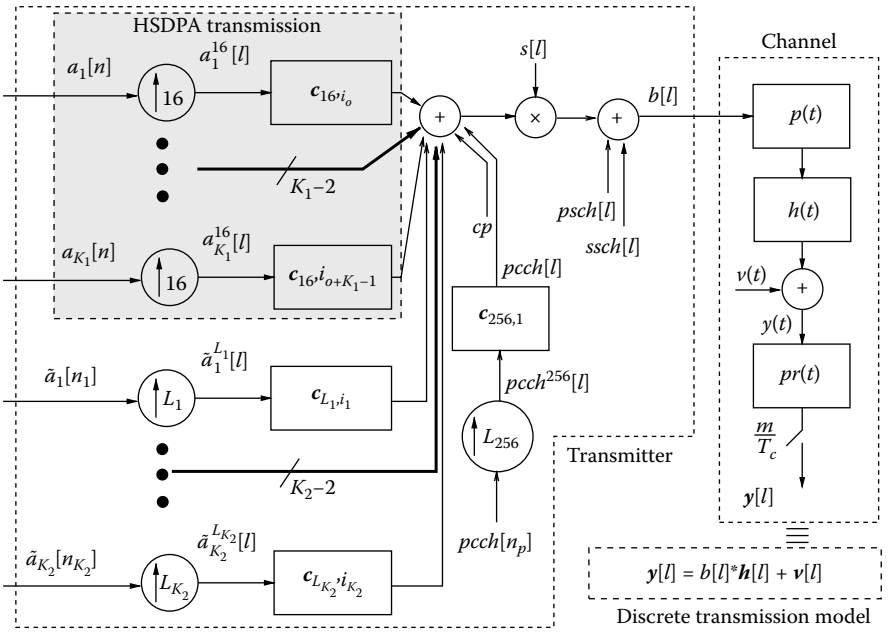

Figure 4.7 Baseband UMTS downlink transmission model.

transmission, are first up-sampled by a factor of 16 and then multiplied with their respective unit-amplitude channelization codes $\{\boldsymbol{c}_{16,i_o}, \boldsymbol{c}_{16,i_o+1}, \ldots, \boldsymbol{c}_{16,i_o+K_1-1}\}$ shown in Figure 4.2. All HSPDSCH symbols have the same power and the same modulation scheme.

The second group of multi-rate transmissions $\{\tilde{a}_1[n_1], \tilde{a}_2[n_2], \ldots, \tilde{a}_{K_2} \times [n_{K_2}]\}$[2] representing the DPCHs, HSSCCHs, and other control channels are similarly up-sampled and convolved with their respective channelization codes:

$$\{\boldsymbol{c}_{L_1,i_1}, \boldsymbol{c}_{L_2,i_2}, \ldots, \boldsymbol{c}_{L_{K_2},i_{K_2}}\}$$

The third group of chip sequences associated with PCCPCH, PCPICH, PSCH, and SSCH channels are denoted as $pcch[l]$, cp, $psch[l]$, and $ssch[l]$, respectively. The common pilot cp symbols are all $\frac{1+j}{\sqrt{2}}$.

The sum of all the generated chip sequences is multiplied with the unit-energy, BS-specific, aperiodic scrambling sequence $s[l]$. PSCH and SSCH are the exceptions, multiplexed after the scrambler, because as a first task

[2] different symbol indices such as $n, n_1, n_2, \ldots, n_{K_2}, n_p$ are used in the text and in Figure 4.7 to stress the *multi-rate* property of the transmission scheme.

in the receiver, they are utilized for determining (i.e., searching), which scrambling sequence is assigned to the BS. The resultant effective BS chip sequence $b[l]$ is transmitted on the channel.

4.3 Downlink Channel and HSDPA Signal Models

UMTS downlink channel has three cascade components: a *root-raised-cosine* (RRC) pulse shape $p(t)$ with a roll-off factor of 0.22, as shown in Figure 4.8; the *time-varying multipath propagation* channel $h(t)$; and a receiver front-end filter $p_r(t)$ that is generally chosen to be again an RRC pulse shape with a roll-off factor of 0.22 due to the fact that the *raised cosine* (rc) result of the 'c' cascade is a *Nyquist pulse* whose T_c-spaced disrete time counterpart is a single unit pulse at time instant 0. In this case, the only source of inter-chip interference (ICI) is $h(t)$. Alternatively, a low-pass anti-aliasing filter with a cutoff frequency between $\frac{1.22}{T_c}$ and $\frac{2}{T_c}$ may be considered as $p_r(t)$ in the case of twice the chip rate sampling. The latter case is a reasonable choice for fractionally spaced equalizers [20,21].

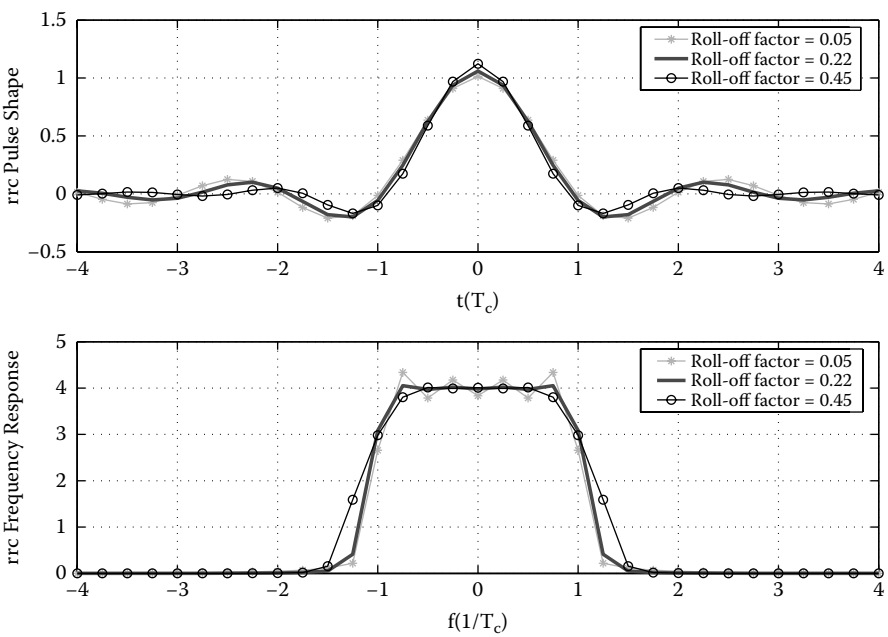

Figure 4.8 Root-raised cosine pulse shapes with different roll-off factors. Higher factors induce less ICI because the tails decay faster but they consume more bandwidth.

The *effective* continuous time channel is hence given as

$$h_{eff}(t) = p(t) * h(t) * p_r(t) \tag{4.2}$$

When there is no transmitter beamforming, the propagation channel and the effective overall channel are unique for all the transmitted code channels from the same BS.

4.3.1 Channel Impairments and Mitigation

Modeling of the propagation channel $h(t)$ is a complex topic in itself [31,32]. We restrict this discussion to intuitive explanations of some aspects that are essential for this chapter.

The most observable effect of the propagation channel on the received signal quality is the time-varying signal amplitude attenuation, which is more often known as *fading* and is a combined consequence of different propagation effects.

The environment-dependent *large-scale* statistics of the UE received power at a distance d (in kilometers) is modeled as[3]

$$P_r \text{ (dBm)} = P_t \text{ (dBm)} - G \text{ (dB)} - 10n\log_{10} d \text{ (dB)} + 10\log_{10} x(dB) \tag{4.3}$$

where P_t is the transmitted power,[4] G is the amount of path loss at a reference distance of 1 km, n is the path loss exponent, and x is the log-normal shadowing term with zero mean and standard deviation σ_x. Shadowing is a consequence of signal absorption by the obstacles in the terrain between the BS and UE, such as hills, trees, buildings, and cars, and it causes a *variance* around the distance-dependent *mean* path loss. It is a *slow-fading* parameter that varies only when the UE changes its position by a distance proportional to the dimensions of an obstructing object.

The most important propagation channel characteristic is the *multipath* effect. Many replicas of the transmitted signal are reflected from several objects and reach the UE with different delays and different complex attenuation factors. Specular replicas are clustered together to generate the effective multi-paths shown in Figure 4.9. The *sparse channel model*, which takes into account only the most dominant P paths, can be formulated as

$$h(t) = \sum_{i=1}^{P} h_i(t)\delta(t - \tau_i(t)) \tag{4.4}$$

The difference between the largest and smallest delay elements, $\Delta_\tau = \tau_P - \tau_1$, is the *delay spread* of the channel. If $\Delta_\tau \geq T_c$, then the channel is

[3] dBm is a relative measure w.r.t. 1 mW power level.

[4] In UMTS terminology, $I_{or} = P_t$ and $\hat{I}_{or} = P_r$.

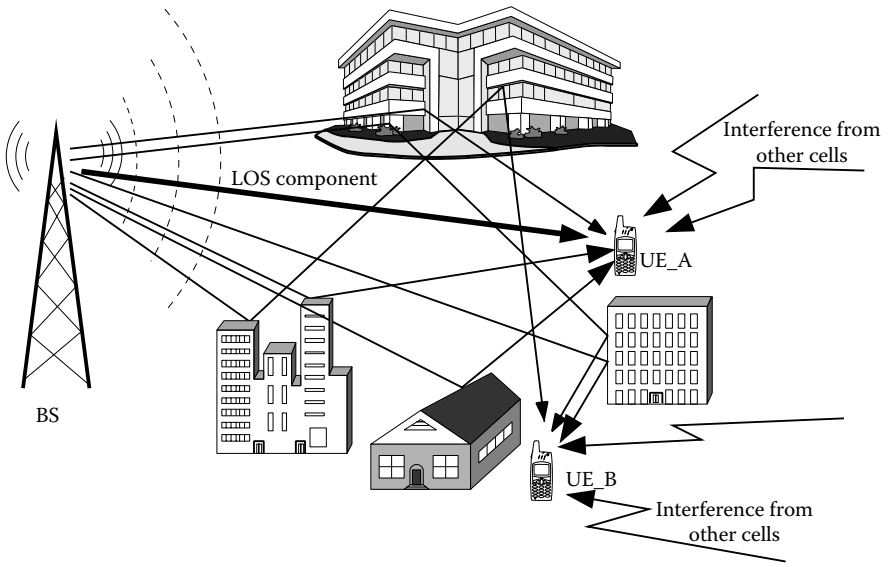

Figure 4.9 Multipath effect.

frequency selective. This comes from the inverse of the delay spread known as *coherence bandwidth* $B_o \approx \frac{1}{\Delta_\tau}$. The physical meaning of B_o is that when two different sinusoidal components with frequencies f_1 and f_2 are transmitted, they are impacted differently by the channel if $\Delta f = |f_1 - f_2| \geq B_o$. In other words, if the signal BW is larger than B_o, which is the case for UMTS *wideband* CDMA downlink, then signal spectrum is nonuniformly affected by the channel. On one hand, if no channel equalization is applied, this is a dispersive situation causing interchip interference (ICI) and driving communication unreliable. On the other hand, it is an opportunity to exploit the inherent *frequency diversity* coming from different subbands of the spectrum, which are considered to be *independently fading*. In the time domain, this property results in the *resolution of the paths* that are separated from each other by at least a distance of T_c. Conventional RAKE receiver exploits frequency diversity by collecting energy via multiple correlations at time instants corresponding to the path delays. Although exact resolution is lower bounded by the chip period, some more diversity is expected from decreasing this constraint to slightly lower values such as $\frac{3T_c}{4}$ [8]. If an opposite situation occurs, that is, if the signal BW is smaller than B_o, then the channel is *flat fading*, meaning that there is no ICI. At first glance this seems to be a good situation not requiring a complicated equalization procedure. However, when there are deep and long-lasting channel fades, as is the case in slow fading channels, other

means such as transmit diversity or receive diversity are necessary to recover from the *outage* state. These techniques, however, complicate BS and UE design.

When all the specular components that generate one dominant path are modeled as i.i.d. complex random variables, then by central limit theorem, channel parameters turn out to be circularly symmetric Gaussian random variables with zero mean and variance $2\sigma_i^2$. Consequently, their complex envelope amplitudes are Rayleigh distributed.

$$p(|h_i(t)|) = \frac{|h_i(t)|}{\sigma_i^2} e^{-\frac{|h_i(t)|^2}{2\sigma_i^2}} \quad \text{for } |h_i(t)| \geq 0, \quad 0 \quad \text{otherwise} \tag{4.5}$$

When there is one very dominant line-of-sight (LOS) path, as is the case for UE_A in Figure 4.9, its distribution is *Rician*, which is more desirable because in that case there are less frequent and less deep fades. In this thesis we are not considering LOS situations.

Sparse multipath channel parameters are modeled as wide-sense stationary and uncorrelated with each other (WSS-US model) [31]. Therefore, each one of them experiences an independent *small-scale* fading due to the movement of the UE, and the movements of the objects that have impacts on that particular path. Previously mentioned shadowing is a *large-scale* complement manifesting itself as birth or death of a path.

The *time-variation* of sparse channel parameters is a metric associated with the amount of signal spectral broadening caused by a Doppler shift, which, in return, is proportional to the *effective* UE velocity in the direction of the coming path ray. The dual relation of a broadening in the frequency domain transfer function is a narrowing of the non-zero channel autocorrelation window in the time domain from infinity to a finite quantity known as channel *coherence time* T_o. The physical meaning of T_o is that when a sinusoid is transmitted twice at times t_1 and t_2, the two are influenced differently by the channel if $\Delta t = |t_1 - t_2| \geq T_o$. The channel is typically considered *fast fading* when $T_o < T_c$ because in this case different parts of a chip are influenced by different-valued channel parameters. With this reasoning, CDMA channels always fall into *slow fading* category. A better criterion to judge whether a channel is fast or slow fading is to compare T_o with the design requirements of the considered application or receiver. If we consider a UE chip equalizer, for example, which recomputes its weights periodically from scratch using the channel estimates, then coherence time should be more than the chosen update period.[5]

[5] A typical requirement for the computation period of nonadaptive HSDPA equalizer weights is 512 chips.

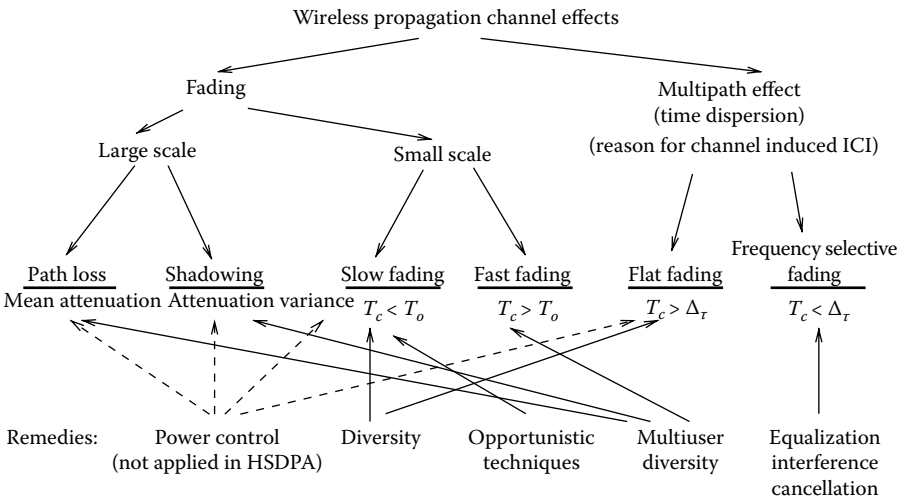

Figure 4.10 Summary of channel impacts and *most relevant* procedures against them.

One might think that slow fading is always a desired situation; however, as explained before, it causes the deep fades to last a long time. In some catastrophic cases, none of the diversity measures will help. Recently some work has been done to mitigate such situations by artificially generating fast-fading channel conditions via a transmission scheme called *opportunistic beamforming* [42].

Figure 4.10 gives a brief summary of the common channel impairments and the principal techniques for mitigating them.

4.3.2 HSDPA Signal Model

The discrete time counterpart of $h_{eff}(t)$ after the sampling operation becomes an FIR *multi-channel* $\boldsymbol{b}[l]$ or equivalently a *poly-phase* channel $\boldsymbol{b}_p[l]$ in the presence of multiple antennas and/or integer factor oversampling w.r.t. the chip rate as is shown in Figure 4.11. In such cases, the received *vector stationary*[6] signal can be modeled as the output of a $m \times 1$ single-input, multi-output (SIMO) system[7] with a past memory of $N-1$ input

[6] Meaning each phase is stationary.

[7] Although stationarity holds only for time-invariant channels, we assume it also for the wireless channels considered in this text, which vary slowly.

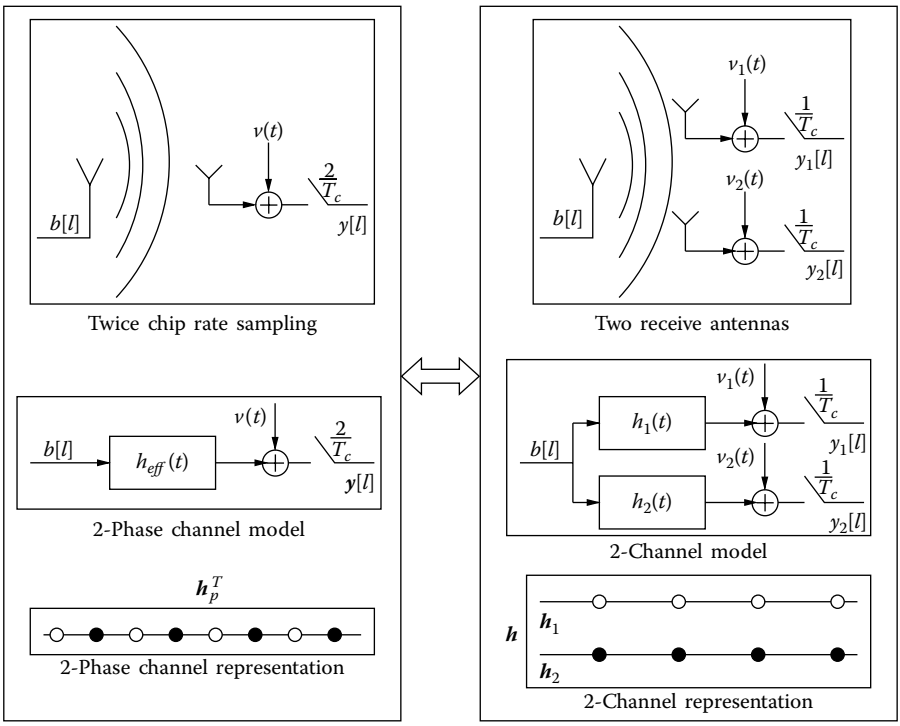

Figure 4.11 The equivalence of the poly-phase and the multi-channel models with a two-phase example. It is possible to pass from one form to the other by P/S and S/P operations.

elements and with the relations

$$\boldsymbol{y}[l] = \sum_{i=0}^{N-1} \boldsymbol{h}[i]b[l-i] + \boldsymbol{v}[l] \tag{4.6}$$

$$\boldsymbol{y}[l] = \begin{bmatrix} y_1[l] \\ \vdots \\ y_m[l] \end{bmatrix}, \quad \boldsymbol{h}[l] = \begin{bmatrix} h_1[l] \\ \vdots \\ h_m[l] \end{bmatrix}, \quad \boldsymbol{v}[l] = \begin{bmatrix} v_1[l] \\ \vdots \\ v_m[l] \end{bmatrix} \tag{4.7}$$

where $\boldsymbol{v}[l]$ denotes the additive noise which represents the sum of the thermal noise and the inter-cell interference filtered by $p_r(t)$, and m denotes the product of the number of antennas and the oversampling factor. The multi-channel $\boldsymbol{h}$ spanning N chips with $m \times 1$ chip rate elements, its poly-phase

equivalent[8] $\boldsymbol{b}_p$, the up-down flipped form $\overline{\boldsymbol{b}}_p$, and the poly-phase matched filter $\boldsymbol{b}_p^{\dagger}$ in row vector format, can be written as

$$\boldsymbol{b} = [\boldsymbol{b}[0], \boldsymbol{b}[1], \ldots, \boldsymbol{b}[N-1]] \tag{4.8}$$

$$\boldsymbol{b}_p = \begin{bmatrix} \boldsymbol{b}[0] \\ \boldsymbol{b}[1] \\ \vdots \\ \boldsymbol{b}[N-1] \end{bmatrix}, \quad \overline{\boldsymbol{b}}_p = \begin{bmatrix} \boldsymbol{b}[N-1] \\ \boldsymbol{b}[N-2] \\ \vdots \\ \boldsymbol{b}[0] \end{bmatrix}, \quad \boldsymbol{b}_p^{\dagger} = \overline{\boldsymbol{b}}_p^{H} \tag{4.9}$$

Assuming $Q-1$ interfering cells, we can write

$$\boldsymbol{y}[l] = \sum_{q=1}^{Q} \sum_{i=0}^{N-1} \boldsymbol{b}^{(q)}[i] b^{(q)}[l-i] + \boldsymbol{v}[l] \tag{4.10}$$

where index $q = 0$ denotes the desired BS.

4.4 Suppression of Intra-cell Interference in HSDPA

Given the channel model discussed above for a single-cell system, we are now ready to discuss some typical receivers for general downlink CDMA systems and, more specifically, HSDPA that are designed to suppress intra-cell interference.

4.4.1 RAKE Receiver and LMMSE Chip Equalizer

As shown in Figure 4.12, all the *linear* UE receivers can be mathematically represented in the form of a common chip-level filter followed by code-specific correlators.[9]

To motivate the discussion of this section, we consider detection of a *single* HSPDSCH user symbol $a_1[0]$ transmitted over the $L \times 1$ channelization code $\boldsymbol{c}_1 = \boldsymbol{c}_{16,0}$.

We consider a two-phase linear filter that has a length of N chips, which is the minimum length to deconvolve, that is, to zero force, a two-phase channel with a length of N chips.

We denote a block of the received signal as $\boldsymbol{Y}$ and denote a block of the *total* transmitted chip sequence as $\boldsymbol{B}$ whose elements are relevant

[8] Represented in column format for compatibility with later formulations.

[9] The order of the correlator and filtering can change, as in the conventional RAKE receiver.

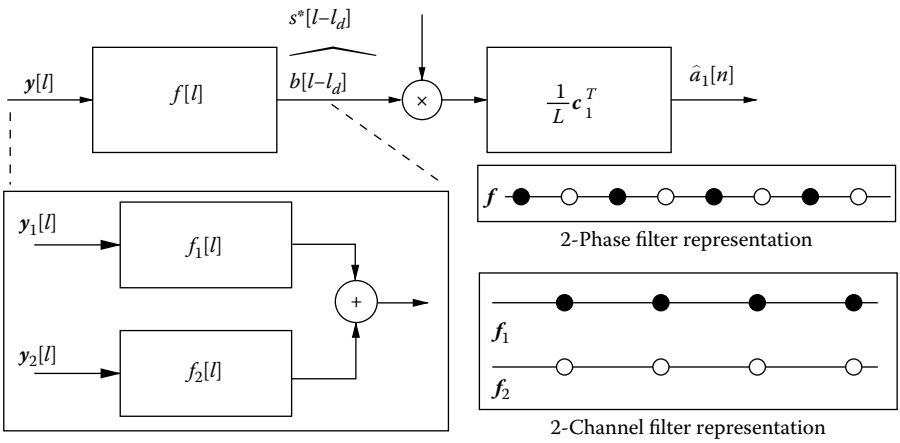

Figure 4.12 Receivers with linear *chip-level filter/correlator* cascade. The order of the phases is reversed w.r.t. the channel phases order.

to the estimation of the latter's subset $\boldsymbol{B}_0 = [b[L-1], \ldots, b[0]]^T$, which overlaps with the period of the $a_1[0]$ symbol. $\boldsymbol{Y}$ and $\boldsymbol{B}$ are related by the $2(L+N-1) \times (L+2N-2)$ channel convolution matrix $\boldsymbol{\mathcal{T}}(\boldsymbol{b})$ with the term $\boldsymbol{V}$, which is modeled as an additive white Gaussian noise (AWGN) representing the sum of the thermal noise and the inter-cell interference.

$$\boldsymbol{Y} = \boldsymbol{\mathcal{T}}(\boldsymbol{b})\boldsymbol{B} + \boldsymbol{V} \tag{4.11}$$

$$= \begin{bmatrix} \boldsymbol{y}[L+N-2] \\ \vdots \\ \boldsymbol{y}[0] \end{bmatrix} \tag{4.12}$$

$$\boldsymbol{\mathcal{T}}(\boldsymbol{b}) = \begin{bmatrix} \boldsymbol{b}[0] & \ldots & \boldsymbol{b}[N-1] & \mathbf{0} & 0 \\ \mathbf{0} & \ddots & \ddots & \ddots & \mathbf{0} \\ 0 & \mathbf{0} & \boldsymbol{b}[0] & \ldots & \boldsymbol{b}[N-1] \end{bmatrix}, \quad \boldsymbol{V} = \begin{bmatrix} \boldsymbol{v}[L+N-2] \\ \vdots \\ \boldsymbol{v}[0] \end{bmatrix} \tag{4.13}$$

$$\boldsymbol{B} = \sum_{k=1}^{K} \left[b_k[L+N-2] \ldots b_k[L-1] \ldots b_k[0] \ldots b_k[-N+1] \right]^T \tag{4.14}$$

K is the number of codes. The linear filter $\boldsymbol{f}[l]$ is a 1×2 multi-input, single-output (MISO) system that turns the overall channel into a single-input,

single-output (SISO) system $\tilde{g}[l]$.

$$\boldsymbol{f} = [\boldsymbol{f}[0], \boldsymbol{f}[1], \ldots, \boldsymbol{f}[N-1]], \quad \boldsymbol{f}[l] = [f[0], f[1]], \quad \tilde{g}[l] = \sum_{i=0}^{l} \boldsymbol{f}[i]\boldsymbol{b}_p[l-i] \tag{4.15}$$

The estimated BS chip sequence $\boldsymbol{B}_0$ can be formulated by the following equations:

$$\widehat{\boldsymbol{B}}_0 = \boldsymbol{\mathcal{T}}(\boldsymbol{f})\boldsymbol{Y} = \boldsymbol{\mathcal{T}}(\boldsymbol{f})\boldsymbol{\mathcal{T}}(\boldsymbol{b})\boldsymbol{B} + \boldsymbol{\mathcal{T}}(\boldsymbol{f})\boldsymbol{V} = \boldsymbol{\mathcal{T}}(\boldsymbol{g})\boldsymbol{B} + \widetilde{\boldsymbol{V}} \tag{4.16}$$

$$\boldsymbol{\mathcal{T}}(\boldsymbol{f}) = \begin{bmatrix} \boldsymbol{f}[0] & \ldots & \boldsymbol{f}[N-1] & \mathbf{0} & 0 \\ \mathbf{0} & \ddots & \ddots & \ddots & \mathbf{0} \\ 0 & \mathbf{0} & \boldsymbol{f}[0] & \ldots & \boldsymbol{f}[N-1] \end{bmatrix}, \quad \widetilde{\boldsymbol{V}} = \begin{bmatrix} \widetilde{v}[L-1] \\ \vdots \\ \widetilde{v}[0] \end{bmatrix} \tag{4.17}$$

$$\boldsymbol{\mathcal{T}}(\boldsymbol{g}) =$$

$$\begin{bmatrix} g[-N+1] & g[-N+2] & \ldots & g[0] & \ldots & g[N-1] & \mathbf{0} & 0 \\ \mathbf{0} & \ddots & \ddots & \ddots & \ddots & \ddots & \ddots & \mathbf{0} \\ 0 & \mathbf{0} & g[-N+1] & g[-N+2] & \ldots & g[0] & \ldots & g[N-1] \end{bmatrix} \tag{4.18}$$

where $\boldsymbol{\mathcal{T}}(\boldsymbol{f})$ denotes the $L \times 2(L+N-1)$ filter convolution matrix, $\boldsymbol{\mathcal{T}}(\boldsymbol{g})$ denotes the $L \times (L+2N-2)$ overall channel convolution matrix, and $g[l] = \tilde{g}[l+N-1]$ reflects a variable change in order to better represent the precursor and postcursor parts of the overall channel, the central tap of which corresponds to $g[0] = \boldsymbol{f}\overline{\boldsymbol{b}}_p$. The channel matched filter (CMF) $\boldsymbol{f} = \overline{\boldsymbol{b}}_p^H$, which is an equivalent of the filtering part of the conventional RAKE receiver, maximizes the SNR, collecting all the channel energy to the central tap as $g[0] = \|\overline{\boldsymbol{b}}_p\|^2 = \|\boldsymbol{b}_p\|^2$. The unbiased form of CMF can be written as

$$\boldsymbol{f} = \left(\boldsymbol{b}_p^H \boldsymbol{b}_p\right)^{-1} \overline{\boldsymbol{b}}_p^H$$

Expanding Equation (4.16), $\widehat{\boldsymbol{B}}_0$ contains every user's chip sequences at different windows, each scaled by the associated tap of the overall

channel

$$\widehat{\boldsymbol{B}}_0 = \sum_{i=-N+1}^{N-1} g[i] \underbrace{\sum_{k=1}^{K} \boldsymbol{B}_{k,i}}_{\boldsymbol{B}_i} + \widetilde{\boldsymbol{V}} \tag{4.19}$$

where $\boldsymbol{B}_{k,i} = [b_k[i+L-1], \ldots, b_k[i]]^T$ and $b_k[i] = a_k\lfloor \frac{i}{L_k} \rfloor c_k[mod(i, L_k)]s[i]$.

The second-stage correlation despreading part of the receiver can be written as

$$\widehat{a_1[0]} = \frac{1}{L}\boldsymbol{c}_1^T \boldsymbol{S}_0^* \widehat{\boldsymbol{B}}_0 \tag{4.20}$$

where $\boldsymbol{S}_i$ denotes a diagonal matrix with the scrambling elements $[s[L-1+i], \ldots, s[i]]$ and the normalization by L is done to make up for the spreading–despreading gain.

Theorem 4.1 *The average SINR of the symbol estimate $\widehat{a_1[0]}$ by the usage of a general chip-level linear filter $\boldsymbol{f}$ is equal to*

$$\Gamma_1 = \frac{L|g(0)|^2\sigma_{b_1}^2}{(\|\boldsymbol{g}\|^2 - |g(0)|^2)\sigma_b^2 + \|\boldsymbol{f}\|^2\sigma_v^2} \tag{4.21}$$

where L is the spreading factor of the first user, $\boldsymbol{g}$ is the impulse response of the channel filter cascade, $\sigma_{b_k}^2$ is the variance of the chips for user k, and $\sigma_b^2 = \sum_{k=1}^{K} \sigma_{b_k}^2$.

Proof. First we give a useful relation:

$$\frac{1}{L}\mathbb{E}\{\boldsymbol{c}_1^T \boldsymbol{S}_0^* \boldsymbol{S}_i \boldsymbol{c}_k^T\} = \begin{cases} 1 & i = 0,\ k = 1 \\ 0 & i = 0,\ k \neq 1 \\ \frac{1}{L} & i \neq 0 \end{cases} \tag{4.22}$$

The symbol estimate can be partitioned into four groups:

$$\widehat{a_1[0]} = \underbrace{g(0)a_1[0]}_{\text{signal}} + \underbrace{\frac{1}{L}\boldsymbol{c}_1^T \boldsymbol{S}_0^* g[0] \sum_{k=2}^{K} \boldsymbol{B}_{k,0}}_{0} + \underbrace{\frac{1}{L}\boldsymbol{c}_1^T \boldsymbol{S}_0^* \left(\sum_{\substack{i=-N+1 \\ i\neq 0}}^{N-1} g[i] \sum_{k=1}^{K} \boldsymbol{B}_{k,i} \right)}_{\text{intracell interference}}$$

$$+ \underbrace{\frac{1}{L}\boldsymbol{c}_1^T \boldsymbol{S}_0^* \widetilde{\boldsymbol{V}}}_{\text{noise}} \tag{4.23}$$

The first component, which represents the useful signal part, is the symbol of interest scaled by the central channel tap $g[0]$. The second component is zero because at the central tap instant $i = 0$, the scrambling and descrambling blocks are aligned, matching each other, $\boldsymbol{S}_0^* \boldsymbol{S}_0 = \boldsymbol{I}_L$, and preserving the orthogonality among users:

$$\boldsymbol{c}_1^T \boldsymbol{S}_0^* \boldsymbol{B}_{k,0} = \boldsymbol{c}_1^T \boldsymbol{S}_0^* \boldsymbol{S}_0 \boldsymbol{c}_k a_k[0] = \boldsymbol{c}_1^T \boldsymbol{c}_k a_k[0] = 0 \quad \forall k \neq 1 \tag{4.24}$$

The third *intra-cell* interference component represents the sum of ICI and MUI (multi-user interference) from the subcomponents with indices $k = 1$ and $k \neq 1$, respectively. The fourth component represents the noise contribution.

Taking the expected value of the symbol estimate power, we obtain

$$\mathbb{E}|\widehat{a}_1[0]|^2 = |g(0)|^2 \sigma_{a_1}^2 + \frac{1}{L} \sum_{\substack{i=-N+1 \\ i \neq 0}}^{N-1} |g[i]|^2 \sum_{k=1}^{K} \sigma_{a_k}^2 + \frac{1}{L} \|\boldsymbol{f}\|^2 \sigma_v^2 \tag{4.25}$$

where $\sigma_{a_k}^2$ represents the symbol variances, the noise power is amplified by the filter energy as is observed in the third component, and the cross terms in the second component disappear due to the expectation relation $\mathbb{E}\{a_k[0] a_l^*[0]\} = 0$, $k \neq l$.

Using the equalities $\|\boldsymbol{f}\|^2 \sigma_v^2 = \boldsymbol{f} \boldsymbol{R}_{vv} \boldsymbol{f}^H$ and $\|\boldsymbol{g}\|^2 = \boldsymbol{f} \boldsymbol{\mathcal{T}}(\boldsymbol{h}) \boldsymbol{\mathcal{T}}(\boldsymbol{h})^H \boldsymbol{f}^H$, $\sigma_{b_k}^2 = \sigma_{a_k}^2$ due to the fact that the channelization codes are not normalized, we obtain

$$\begin{aligned} \mathbb{E}|\widehat{a}_1[0]|^2 &= |g(0)|^2 \sigma_{a_1}^2 + \frac{1}{L} (\|\boldsymbol{g}\|^2 - |g(0)|^2) \sigma_b^2 + \frac{1}{L} \|\boldsymbol{f}\|^2 \sigma_v^2 \\ &= |g(0)|^2 \sigma_{a_1}^2 + \frac{1}{L} \boldsymbol{f} \left(\underbrace{\sigma_b^2 \boldsymbol{\mathcal{T}}(\boldsymbol{h}) \boldsymbol{\mathcal{T}}(\boldsymbol{h})^H + \boldsymbol{R}_{vv}}_{\boldsymbol{R}_{yy}} \right) \boldsymbol{f}^H - \frac{1}{L} |g(0)|^2 \sigma_b^2 \end{aligned}$$

Accordingly, we reach the SINR expression:

$$\Gamma_1 = \frac{|g(0)|^2 \sigma_{a_1}^2}{\frac{1}{L} (\|\boldsymbol{g}\|^2 - |g(0)|^2) \sigma_b^2 + \frac{1}{L} \|\boldsymbol{f}\|^2 \sigma_v^2} \tag{4.26}$$

$$= \frac{|g(0)|^2 \sigma_{b_1}^2}{\frac{1}{L} (\|\boldsymbol{g}\|^2 - |g(0)|^2) \sigma_b^2 + \frac{1}{L} \|\boldsymbol{f}\|^2 \sigma_v^2} \tag{4.27}$$

$$= \frac{L |g(0)|^2 \sigma_{b_1}^2}{\boldsymbol{f} \boldsymbol{R}_{yy} \boldsymbol{f}^H - |g(0)|^2 \sigma_b^2} \tag{4.28}$$

□

Although the SINR expression is for symbol estimation, in reality the linear filter $\boldsymbol{f}$ estimates the BS chip sequence $b[l]$. Therefore, the modified SINR expression for the estimation of the BS chip sequence can be written as

$$\Gamma_c = \frac{|g(0)|^2\sigma_b^2}{\boldsymbol{f}\boldsymbol{R}_{yy}\boldsymbol{f}^H - |g(0)|^2\sigma_b^2} \tag{4.29}$$

where at the numerator (i.e., the useful energy part), there is no spreading gain and $\sigma_{b_1}^2$ is replaced by σ_b^2.

The SINR metrics in Equations (4.26) and (4.29) are based on the estimation of $\boldsymbol{R}_{yy}$ statistics by taking expectation over the scrambler, which is modeled as a random sequence, and using the orthogonality property of the codes. The receiver that maximizes these SINR metrics is the Max-SINR receiver, which is more often known as the chip-level LMMSE (linear minimum mean square error) receiver [20,21].

Theorem 4.2 *The unbiased linear filter which maximizes SINR without exploiting the code and the power knowledge of the active users but by modeling the scrambling sequence as a random sequence and by taking expectations over it to approximate the received signal covariance matrix* $\boldsymbol{R}_{yy}$ *is equal to [21]*

$$\boldsymbol{f}_o = \left(\overline{\boldsymbol{b}}_p^H\boldsymbol{R}_{yy}^{-1}\overline{\boldsymbol{b}}_p\right)^{-1}\overline{\boldsymbol{b}}_p^H\boldsymbol{R}_{yy}^{-1} \tag{4.30}$$

Proof. We first define the unbiasedness constraint as $g[0] = \boldsymbol{f}_o\overline{\boldsymbol{b}}_p = 1$. Then the optimization problem can be formulated as

$$\boldsymbol{f}_o = \arg_{\boldsymbol{f}} \max_{\boldsymbol{f}_o\overline{\boldsymbol{b}}_p=1} \Gamma_1 = \arg_{\boldsymbol{f}} \min_{\boldsymbol{f}_o\overline{\boldsymbol{b}}_p=1} \boldsymbol{f}\boldsymbol{R}_{yy}\boldsymbol{f}^{\boldsymbol{H}} \tag{4.31}$$

The solution can be obtained by the standard Lagrange multiplier technique as follows:

$$\Omega(\boldsymbol{f}^H, \boldsymbol{f}) = \boldsymbol{f}\boldsymbol{R}_{yy}\boldsymbol{f}^{\boldsymbol{H}} + 2\Re[\lambda(\boldsymbol{f}\overline{\boldsymbol{b}}_p - 1)]$$

$$\nabla_{\boldsymbol{f}}\Omega(\boldsymbol{f}^H, \boldsymbol{f}) = \boldsymbol{f}\boldsymbol{R}_{yy} + \lambda\overline{\boldsymbol{b}}_p^H$$

$$\Rightarrow \boldsymbol{f}_o = -\lambda\overline{\boldsymbol{b}}_p^H\boldsymbol{R}_{yy}^{-1}$$

$$\boldsymbol{f}_o\overline{\boldsymbol{b}}_p = 1 \Rightarrow -\lambda\overline{\boldsymbol{b}}_p^H\boldsymbol{R}_{\boldsymbol{y}y}^{-1}\overline{\boldsymbol{b}}_p = 1$$

$$\Rightarrow \lambda = \frac{-1}{\overline{\boldsymbol{b}}_p^H\boldsymbol{R}_{\boldsymbol{y}y}^{-1}\overline{\boldsymbol{b}}_p}$$

$$\Rightarrow \boldsymbol{f}_o = \frac{\overline{\boldsymbol{b}}_p^H\boldsymbol{R}_{\boldsymbol{y}y}^{-1}}{\overline{\boldsymbol{b}}_p^H\boldsymbol{R}_{\boldsymbol{y}y}^{-1}\overline{\boldsymbol{b}}_p} = \frac{\boldsymbol{b}_p^\dagger\boldsymbol{R}_{\boldsymbol{y}y}^{-1}}{\boldsymbol{b}_p^\dagger\boldsymbol{R}_{\boldsymbol{y}y}^{-1}\overline{\boldsymbol{b}}_p}$$

□

By taking an approximation of Equation (4.30), we can obtain the biased (but simpler) chip-level LMMSE filter:

$$\tilde{\boldsymbol{f}}_o = \sigma_b^2\boldsymbol{b}_p^\dagger\boldsymbol{R}_{\boldsymbol{y}y}^{-1} = \boldsymbol{R}_{b\boldsymbol{y}}\boldsymbol{R}_{\boldsymbol{y}y}^{-1} \tag{4.32}$$

which fits the Wiener filtering format.

Similar to the update from Equations (4.6) to (4.10), if one has channel estimates of some other cells, then a better performing chip equalizer expression can be obtained as

$$\tilde{\boldsymbol{f}}_o = \sigma_{b^{(0)}}^2\boldsymbol{b}_p^{(0)\dagger}\left(\sum_{q=0}^{Q-1}\sigma_{b^{(q)}}^2\boldsymbol{\mathcal{T}}(\boldsymbol{b}^{(q)})\boldsymbol{\mathcal{T}}(\boldsymbol{b}^{(q)})^H + \boldsymbol{R}_{vv}\right)^{-1} \tag{4.33}$$

by modifying the $\boldsymbol{R}_{\boldsymbol{yy}}$ term.[10]

4.4.2 HSDPA Performance Analysis of RAKE Receiver and Chip Equalizers

In this section we obtain the maximum achievable SINR and throughput performance metrics for various HSDPA service deployment scenarios while using the CMF and LMMSE equalizer-type UE receivers. The distributions of the radio channel parameters and the received powers from the own and surrounding base stations are modeled under correlated shadowing w.r.t. the mobile position, the cell radius, and the type of environment. From such modeling, more realistic performance figures might be obtained as compared to fixing them to a selected set of values.

[10] This equalizer has the inter-cell interference suppression capability, which will be further elaborated in later parts of this chapter.

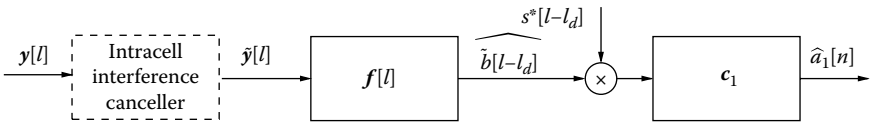

Figure 4.13 Hypothetical receiver model.

4.4.2.1 Hypothetical Receiver Models

We consider that possibly an interfering cancelling (IC) structure is used in the first stage to cancel out intra-cell interference contributions of the PCPICH and HSPDSCHs (Figure 4.13).

We assume that the residual BS signal $\tilde{b}[l]$ contained in the remaining sequence $\tilde{\boldsymbol{y}}[l]$ after the IC block is still block stationary and the second-order inter-cell interference plus noise statistics σ_v^2 are the same as before.

The modified SINR expression at the unbiased linear filter output (i.e., when $g[0] = 1$), for the symbol estimates of a single HSPDSCH channel of a UE situated at a particular position of the cell can be written as

$$\Gamma_1 = \frac{16\rho P_0}{(\frac{1}{\alpha} - 1)\chi P_0 + \sum_{i=1}^{6} P_i \|\boldsymbol{g}_i\|^2 + \|\boldsymbol{f}\|^2 \sigma_n^2} \tag{4.34}$$

where 16 is the HSPDSCH spreading gain, P_0 is the received power of the desired BS (BS 1), there are K_1 HSPDSCH codes, ρ is the BS signal power portion of one HSPDSCH channel, χ is the remaining BS signal power portion after the IC block, P_i is the received powers from the ith cell among the six first-tier interfering unsectored cells[11] shown in Figure 4.1, $\boldsymbol{g}_i$ is the convolution of the linear filter $\boldsymbol{f}$ and the channel $\boldsymbol{h}_i$ originating from the ith surrounding cell as $\boldsymbol{g}_i = \boldsymbol{f} * \boldsymbol{h}_i$, and σ_n^2 is the AWGN variance. The AWGN term and inter-cell interference are treated separately for performance analysis purposes, whereas they are treated similarly for filter adaptation due to the fact that it is impractical to incorporate in the signal model channel estimates and signal variances for a large number (six here) of neighboring cells. As shown in the example of channel and CMF impulse responses in Figure 4.14, the term $\alpha = \frac{1}{\|\boldsymbol{g}\|^2}$ represents the ratio of the useful effective channel energy to the total effective channel energy and is known as the *orthogonality factor*, which was previously treated in the literature only for the RAKE receiver variants [25,29].

[11] The analysis done in this chapter is also valid for the sectored case.

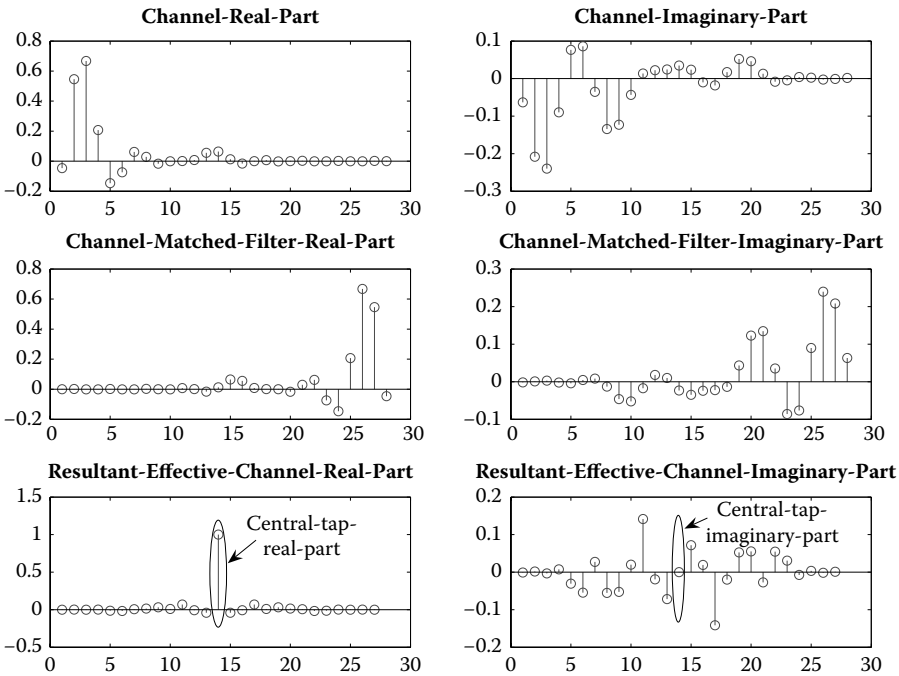

Figure 4.14 Orthogonality factor representation over an unbiased CMF. The central tap of the effective channel collects all the energy, which is 1 due to unbiasedness. The cumulative energy of all the taps is $\|\boldsymbol{g}\|^2$.

4.4.2.2 Parameter Modeling

We model all the parameters that appear in the SINR expression and that implicitly or explicitly depend on one or more of the locations of the UE in the cell, the radius (r) of the cell, and the type of environment.

4.4.2.2.1 Modeling Received Powers

Received powers are calculated by the path loss and shadowing computations discussed previously. For shadowing we first randomly generate a vector of seven independent shadowing values $\tilde{\boldsymbol{x}}$ of the own and first-tier six cells and turn it into a cross-correlated vector $\boldsymbol{x}$ by left multiplying with the lower triangular Cholesky factorization output matrix $\boldsymbol{L}_{\boldsymbol{x}}$ of the symmetric shadowing correlation matrix $\boldsymbol{R}_{\boldsymbol{xx}}$ whose elements $\rho_{x_i x_j}$ given in Table 4.1 are obtained from the distance ratio dr_{ij} and the angle values θ_{ij}

Table 4.1 Shadowing Correlation Matrix Elements

	$0 < \theta_{ij} < 30^\circ$	$30^\circ \leq \theta_{ij} < 60^\circ$	$60^\circ \leq \theta_{ij} < 90^\circ$	$90^\circ \leq \theta_{ij}$
$dr_{ij} \in [0, 2]$	$\rho_{x_i x_j} = 0.8$	$\rho_{x_i x_j} = 0.5$	$\rho_{x_i x_j} = 0.4$	$\rho_{x_i x_j} = 0.2$
$dr_{ij} \in [2, 4]$	$\rho_{x_i x_j} = 0.6$	$\rho_{x_i x_j} = 0.4$	$\rho_{x_i x_j} = 0.4$	$\rho_{x_i x_j} = 0.2$
$dr_{ij} \geq 4$	$\rho_{x_i x_j} = 0.4$	$\rho_{x_i x_j} = 0.2$	$\rho_{x_i x_j} = 0.2$	$\rho_{x_i x_j} = 0.2$

between the corresponding couples among the seven BSs and the UE as shown in Figure 4.15 [46].

$$\boldsymbol{R_{xx}} = \begin{bmatrix} \rho_{x_0,x_0} & \rho_{x_0,x_1} & \cdots & \rho_{x_0,x_6} \\ \rho_{x_1,x_0} & \rho_{x_1,x_1} & \cdots & \rho_{x_1,x_6} \\ \vdots & \vdots & \vdots & \vdots \\ \rho_{x_6,x_0} & \rho_{x_6,x_1} & \cdots & \rho_{x_6,x_6} \end{bmatrix} = \boldsymbol{L_x L_x}^T, \quad \boldsymbol{x} = \boldsymbol{L_x \tilde{x}} \tag{4.35}$$

4.4.2.2.2 Modeling Channel Parameters

The linear filter $\boldsymbol{f}$, the orthogonality factor α, and the $\boldsymbol{g}_i$ terms depend on the channel parameters, for which we refer to Greenstein's channel model derived from the rms delay spread σ_{τ_i} and the power delay profile $P(\tau_i)$ [16]. Delay spread is equal to $\sigma_{\tau_i} = T_1 d^{\epsilon} y_i$, where T_1 is the reference delay spread at 1-km distance from the BS; ϵ is the model parameter, which is around 0.5 for almost all types of environments except very irregular mountainous terrains; and y_i is a coefficient, which is log-normally distributed with geometric mean 0 and geometric standard deviation σ_{y_i}. From field tests, $\log(y_i)$ is also observed to be correlated with $\log(x_i)$ by a factor $\rho_{x_i y_i} = -0.75$ [16]. So we obtain the value of y_i from the correlation with the obtained shadowing value in the previous section. From the obtained delay spread we generate the power delay profile as $P(\tau_i) \propto e^{-\tau_i/\sigma_{\tau_i}}$ where $\propto$ is

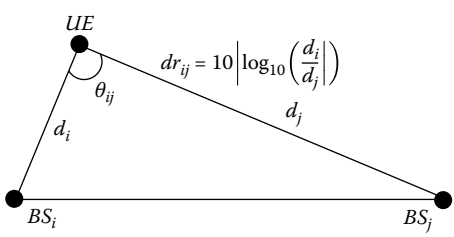

Figure 4.15 Distance and angle relations between two BSs and a UE.

the proportionality sign and τ_i values are the sampling instants. Because this is an infinite-length sequence, we truncate it at the position where the final significant tap has 15 dB less power than the first tap. Then we pass the discrete power delay profile through *Rayleigh* fading to generate the *propagation* channel. The *transmission* channels are obtained by convolving the obtained propagation channels with the pulse shape and normalizing the result to unit energy.

4.4.2.2.3 Modeling χ

Among the common downlink channels, the pilot tone PCPICH has the highest interference with 10% BS power portion and it can be cancelled with high accuracy [35]. However, it might be even more meaningful to consider cancelling the interference of HSPDSCH codes because, by a highly probable deployment scenario, they will carry the majority (if not all) of the data traffic. We contemplate this because it would be easier to manage for an operator to dedicate one of its two or three carriers of 5 MHz to the HSDPA service instead of distributing it over two or three available carriers. Furthermore, there is no justified advantage of carrying high-rate data on a DCH with a very low spreading factor instead of on multiple HSPDSCHs. So, in the reception chain for a single HSPDSCH, we define five *perfect* first-stage interference cancellation (IC) scenarios:

1. No interference canceller exists: $\chi = 1$
2. Pilot tone cancelled: $\chi = 0.9$
3. All the other HS-PDSCHs cancelled: $\chi = 1 - (K_1 - 1)\rho$
4. Pilot+HS-PDSCHs cancelled: $\chi = 0.9 - (K_1 - 1)\rho$
5. All intra-cell interference cancelled: $\chi = \rho$

4.4.2.3 Simulations Results

Five different environments are considered, the relevant parameters of which are shown in Table 4.2 and adopted from COST231 propagation

Table 4.2 Cellular Deployment Scenarios

Parameters	G_1	n	r	T_1	σ_x	σ_y
Indoor	138	2.6	0.2	0.4	12	2
Urbanmicro	131	3	0.5	0.4	10	3
Urbanmacro	139.5	3.5	1	0.7	8	4
Suburbanmacro	136.5	3.5	2	0.3	8	5
Rural	136.5	3.85	8	0.1	6	6

models [34] and from [16]. We fix the transmitted BS power and AWGN power to $P_t = 43$ dBm and $\sigma_n^2 = -102$ dBm, respectively. Three different low-end to high-end HSDPA service scenarios are considered with $\{K_1, \rho\}$ set as $\{1, 0.1\}$, $\{5, 0.06\}$, and $\{10, 0.06\}$. We uniformly position 10^4 UEs in one cell (home cell) and approximately that many more in an expanded region penetrating into other cells. This models the effect of shadowing, resulting in handing off some UEs to other base stations depite their relatively greater distance as compared to the BS closest to the user. We also exclude a few closest points to the BS because otherwise, the BS will serve only the closest UEs. For each node receiving the highest power from the BS of interest, we determine the relevant second-order statistics over ten Rayleigh fading channel realizations. At each realization we obtain the SINR and spectral efficiency bound $\mathcal{C} = \log_2(1 + \Gamma_1)$ results for the CMF and LMMSE equalizer-correlator type receivers under the five above-mentioned interference cancellation scenarios. It was shown that the interference at the output of multi-user detectors can be approximated by a Gaussian distribution [30,47]. Hence, $\mathcal{C}$ is an approximate Shannon capacity and is a more meaningful measure than SINR because it defines the overall performance bound that can be achieved by the use of efficient transmission diversity, modulation, and channel coding schemes. A number of spatiotemporal results on the order of 10^5 suffices to obtain the distribution of $\mathcal{C}$. Cumulative distributions of $\mathcal{C}$ for ten HSPDSCH codes deployment in the five reference environments are shown in Figures 4.16 through 4.20. The calculated median values of $\mathcal{C}$ for all the settings defined are tabulated in Table 4.3.

In the figures and the table, C represents CMF; E represents LMMSE equalizer-correlator receiver; suffixes to C and E ($\{1, \ldots, 5\}$) represent (in the same order) the IC scenarios defined in section 4.4.2.2.3; {ind, umi, uma, sub} represent {indoor, urban microcell, urban macrocell, suburban macrocell} environments; and the suffixes {1, 5, 10} to these environments represent K_1.

As observed in the figures, an increasing gap occurs between matched filtering results and equalization results when we go to user locations closer to the own BS, which correspond to higher SINR regions. This is especially the valid case for indoor cells, urban microcells, and urban macrocells, where the eye is open for all user locations because white noise (thermal noise and partially inter-cell interference) suppressing CMF is much more affected by intra-cell interference, most of which, however, is suppressed when an equalizer is used and the need for an IC decreases. In other words, in such environments, orthogonality factors at the output of LMMSE equalizers are much higher than those of CMFs.

In the suburban macrocell sizes, for the most distant 30% cellular positions, there is no difference in the performance of receivers. When we go farther to the extreme rural cell sizes, there is almost no difference except at a small number of very close UE positions. These figures clearly show

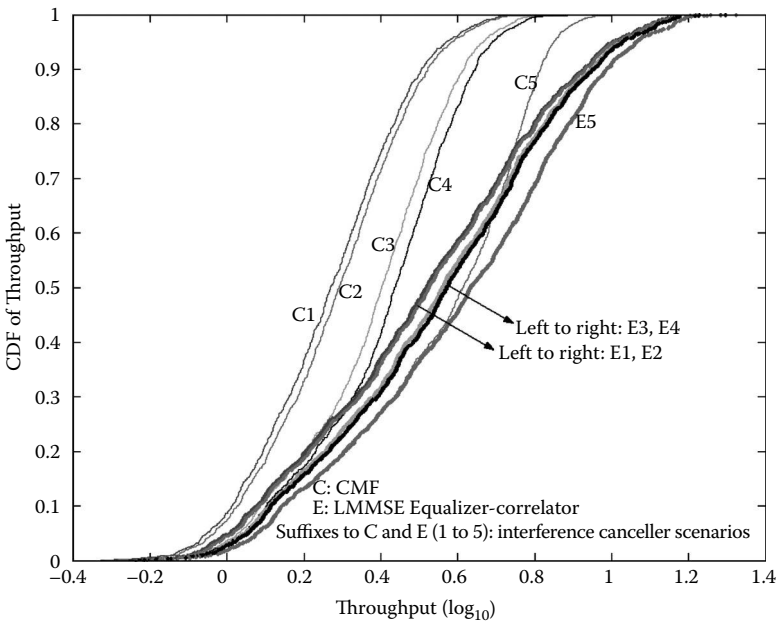

Figure 4.16 Throughput bound CDF of indoor microcell. Number of codes = 10; total HSDPA power portion = 0.6.

the dominance of multi-user interference in small cells where using interference suppressing equalizers becomes meaningful and the dominance of AWGN in the large cells where CMF or RAKE receiver is sufficient.

According to UMTS deployment scenarios, more than 80% of UMTS cells will be pico- or microcells, and hence it will certainly pay off if a UE considers the LMMSE equalizer in order to be scheduled for a high-SINR-demanding HSDPA service. In these settings, the achievable *maximum* $\mathcal{C}$ using equalizers is approximately twice that of CMFs. So, under ideal conditions, CMF has less chance of providing a very high-rate-demanding application.

In Table 4.3, we notice that when an equalizer is used, the median capacity for a UE increases when we move from indoor to urban environments, which is mostly because of the trend of the path-loss exponent. When it is low, inter-cell interference will be high. However, as we further increase the size of the cell, AWGN starts to dominate and median capacity decreases. We also see that w.r.t. CMF, equalizers alone improve the median capacity of pico- and microcells between 60% and 115%. When

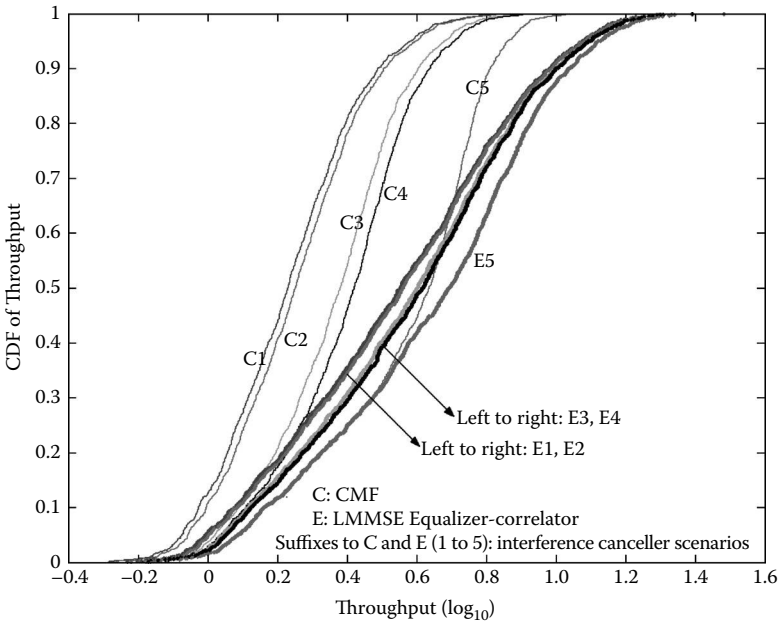

Figure 4.17 Throughput bound CDF of urban microcell. Number of codes = 10; total HSDPA power portion = 0.6.

complete interference cancellation is achieved, these figures increase to 98% and 199%.

Cancelling the pilot tone alone brings very little gain. Moshavi et al., however, claim that it is possible to obtain 11% capacity gain by cancelling the 10% power pilot tone because this much cancelled power can be exploited by the BS to accept a proportional number of new users [36]. This can be valid only if all the UE receivers at the same time cancel the pilot tone, which is not dictated for the moment by the standard. Nevertheless, when equalization is used, it is more worthwhile to subtract known non-orthogonal channels (e.g., the synchronization channels). We, however, will not discuss this aspect any further due to space limitations.

Note that the results obtained are valid when there is no LOS and surrounding cells have identical properties. In reality, we expect higher capacity from picocellular regions because there will be some isolated hot zones like airports and there will be a higher probability of LOS. Furthermore, note that the capacity we are concerned with here is the single-cell capacity. Of course, global system capacity from the adoption of picocells will

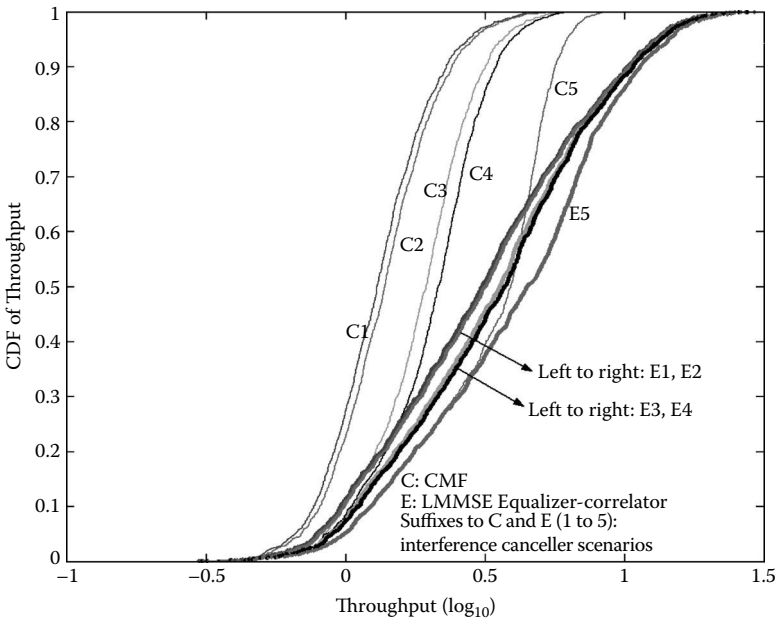

Figure 4.18 Throughput bound CDF of urban macrocell. Number of codes = 10; total HSDPA power portion = 0.6.

be much higher than others because there will be more cells and hence more users will be served.

4.5 Advanced Receivers for Interference Cancellation

Chip-level equalization happens to be a solution of interest for the very specific case of downlink synchronous CDMA. When multi-user interference is of a more general nature (e.g., due to asynchronous or non-orthogonal downlink codes), the solutions for its suppression are equivalently more general and are labeled *multi-user* receivers or detectors. We discuss some well-documented multi-user receivers in this section and later apply them to the specific case of suppression of inter-cell interference in the HSDPA downlink.

4.5.1 Symbol-Rate Signal Model

The signal model in Equation (4.10) is a chip-rate model where $b^{(q)}[i]$ is the ith chip from the qth base station. We can write the equivalent discrete-time

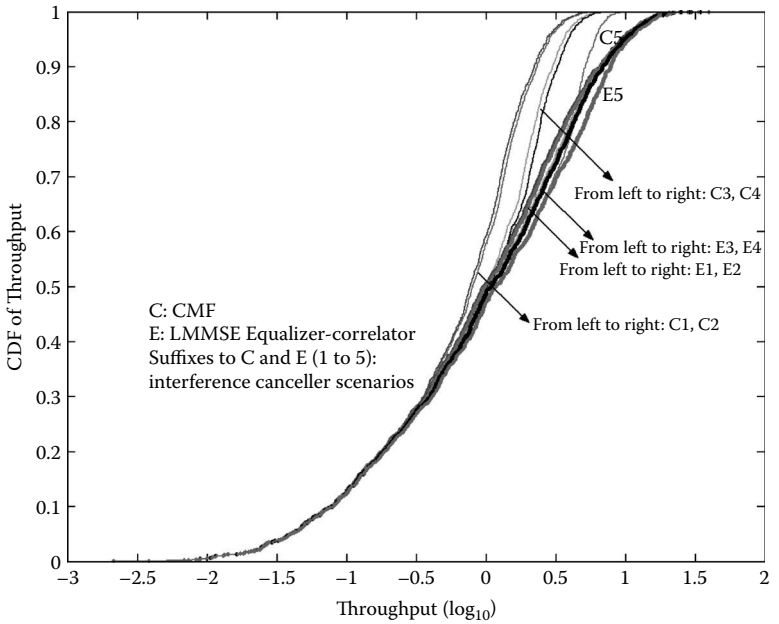

Figure 4.19 Throughput bound CDF of suburban macrocell. Number of codes = 10; total HSDPA power portion = 0.6.

signal model at the symbol-rate as

$$\boldsymbol{Y}[n] = \sum_{q=0}^{Q-1} \overbrace{\boldsymbol{\mathcal{T}}(\boldsymbol{h}^{(q)})\boldsymbol{S}^{(q)}[n]\boldsymbol{C}}^{\tilde{\boldsymbol{G}}^{(q)}[n]} \boldsymbol{A}^{(q)}[n] + \boldsymbol{V}[n] \tag{4.36}$$

where K is the number of users assumed without loss of generality the same from all base stations, $\boldsymbol{Y}[n]$ represents the received data block spanning the channel output corresponding to transmission of M symbols at time instant n, $\tilde{\boldsymbol{G}}^{(q)}[n]$ is the symbol-rate channel[12] from base station q composed of the cascade of the propagation channel $\boldsymbol{\mathcal{T}}(\boldsymbol{h}^{(q)})$, the diagonal scrambling code matrix $\boldsymbol{S}^{(q)}[n]$, and the block-diagonal channelization code matrix $\boldsymbol{C}$, assumed to be the same for all base stations. $\boldsymbol{A}^{(q)}[n]$ represents the unit-amplitude MK desired symbols vector. Because the nature of intra-cell and inter-cell interference is the same (non-orthogonal), we assume, in the interest of clarity, only one base station $Q = 1$ and suppress the index q for the purposes of the following discussion.

[12] Time-varying because it includes the scrambler.

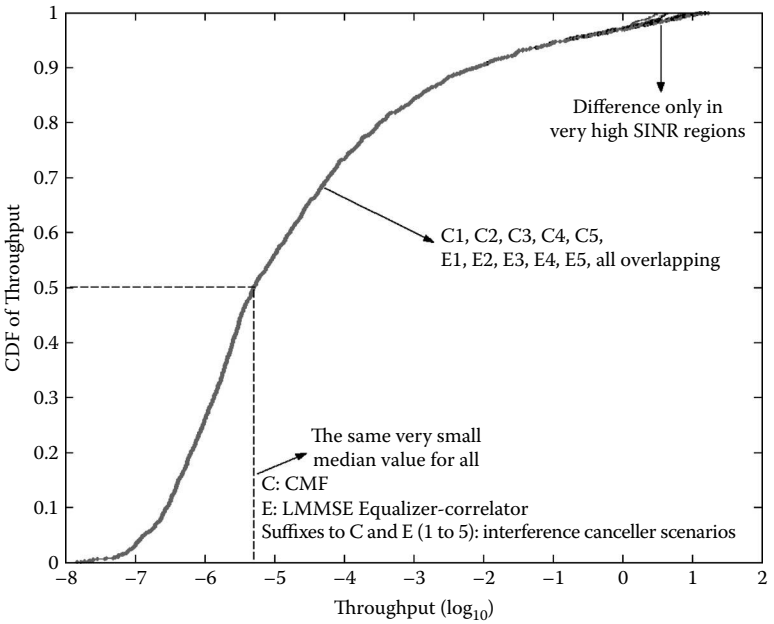

Figure 4.20 Throughput bound CDF of rural cell. Number of codes = 10; total HSDPA power portion = 0.6.

4.5.2 Optimal Receiver

The optimal multi-user detector in terms of minimum symbol error rate (SER) is the Maximum Likelihood Sequence Estimation (MLSE), which is an exhaustive search procedure over the symbol alphabets of all the possible transmitted sequences of all the users with the minimization criterion [22]

$$\hat{\boldsymbol{A}}_{ML} = \arg \min_{\boldsymbol{A} \in \mathcal{X}^{MK}} \left\| \boldsymbol{Y} - \overbrace{\boldsymbol{\mathcal{T}}(\boldsymbol{h})\boldsymbol{S}\boldsymbol{C}}^{\tilde{\boldsymbol{G}}} \boldsymbol{A} \right\|^2 \tag{4.37}$$

where $\mathcal{X}$ denotes the symbol alphabet.[13] Because this criterion is finite-alphabet constrained, it is NP-hard[14] and perhaps the best that can be done is to use the Viterbi algorithm, which is also exponentially complex with

[13] Representing the simple case of same constellation for all users.

[14] A decision problem that is at least as hard as any problem whose solution can be *verified* by polynomial complexity.

Table 4.3 Throughput Bound Median Results

$\mathcal{C}$	C1	C2	C3	C4	C5	E1	E2	E3	E4	E5
ind1	2.46	2.54	2.46	2.54	4.54	3.94	3.99	3.94	3.99	4.87
ind5	1.86	1.94	2.09	2.21	4.13	3.22	3.27	3.33	3.42	4.34
ind10	1.86	1.96	2.53	2.73	4.11	3.31	3.35	3.63	3.73	4.30
umi1	2.18	2.29	2.18	2.29	4.54	4.16	4.20	4.16	4.20	5.30
umi5	1.65	1.74	1.89	2.02	4.34	3.56	3.59	3.71	3.77	4.94
umi10	1.70	1.79	2.41	2.63	4.32	3.59	3.63	4.00	4.16	4.95
uma1	1.78	1.88	1.78	1.88	4.13	3.80	3.86	3.80	3.86	5.16
uma5	1.30	1.37	1.50	1.62	3.97	3.09	3.14	3.26	3.35	4.72
uma10	1.30	1.38	1.95	2.15	3.91	3.10	3.17	3.58	3.74	4.50
sub1	1.11	1.17	1.11	1.17	1.60	1.40	1.42	1.40	1.42	1.61
sub5	0.79	0.82	0.87	0.91	1.19	1.02	1.03	1.05	1.06	1.19
sub10	0.77	0.81	0.97	1.02	1.18	0.98	1.00	1.07	1.09	1.18

the factor MK [44]. Due to these reasons, the ML (Maximum Likelihood) receiver is mostly considered not implementable and its performance serves only as an upper bound. Furthermore, in case of signals from multiple base stations, ML detection of all symbols from all base stations must be considered, making the solution even more undesirable in the downlink problem. Note that Equation (4.37) is at the same time the nonlinear LS estimator.[15]

4.5.3 Decorrelating Receiver

One of the suboptimal but simpler approaches is to relax the finite-alphabet constraint mapping of $\boldsymbol{A}$ from the finite set $\mathcal{X}^{MK}$ into $\mathbb{C}^{MK}$, which turns the nonlinear LS problem in Equation (4.37) into a linear LS problem:

$$\hat{\boldsymbol{A}}_{LS} = \arg \min_{\boldsymbol{A} \in \mathbb{C}^{MK}} \|\boldsymbol{Y} - \tilde{\boldsymbol{G}}\boldsymbol{A}\|^2 \tag{4.38}$$

[15] In statistical terms, LS is *disguised* ML when the measurement noise sequence $\boldsymbol{V}$ is zero-mean, *i.i.d.*, and Gaussian.

whose solution is

$$\hat{\boldsymbol{A}}_{LS} = \tilde{\boldsymbol{F}}_{Dec}\boldsymbol{Y} = \left(\overbrace{\tilde{\boldsymbol{G}}^{H}\tilde{\boldsymbol{G}}}^{\boldsymbol{R}}\right)^{-1} \tilde{\boldsymbol{G}}^{H}\boldsymbol{Y} = \boldsymbol{R}^{-1}\boldsymbol{X} \tag{4.39}$$

where $\boldsymbol{X}$ and $\boldsymbol{R}$, respectively, denote the single-user, matched-filter (SUMF) bank output symbol estimates and their cross-correlation matrix.

An equivalent model in terms of linear systems of equations can be written as

$$\boldsymbol{R}\hat{\boldsymbol{A}}_{LS} = \boldsymbol{X} \tag{4.40}$$

Note that the LS estimator treats the elements of $\boldsymbol{A}$ vector as deterministic unknown parameters having diffuse prior pdfs.

LS estimation (i.e., decorrelation) is the unique least MSE member of the ZF (zero forcing) MUD (multi-user diversity gains, thus called MMSE-ZF receiver) set with the general members expressed as

$$\hat{\boldsymbol{A}}_{ZF} = (\boldsymbol{T}\tilde{\boldsymbol{G}})^{-1}\boldsymbol{T}\boldsymbol{Y}$$

with any proper $\boldsymbol{T}$ matrix.

4.5.3.1 Projection Interpretation of Decorrelating Receiver

Projection receiver is another name for the symbol-level MMSE-ZF. It was first presented as the projection receiver for CDMA communications by Schlegel et al. [37] and is based on suppressing both inter-cell and intra-cell interference by projecting the undesired users onto the subspace orthogonal to the one spanned by the desired user's signal vector. We propose different approaches for both exact and approximated interference projection.

Considering the symbol-level model,

$$\boldsymbol{Y}[n] = \tilde{\boldsymbol{G}}[n]\boldsymbol{A}[n] + \boldsymbol{V}[n] \tag{4.41}$$

We call $d[n]$ the symbol to estimate, $\tilde{\boldsymbol{g}}[n]$ the column of $\tilde{\boldsymbol{G}}[n]$ corresponding to that symbol, and $\bar{\boldsymbol{G}}[n]$ all the other columns of $\tilde{\boldsymbol{G}}[n]$. Inter-symbol interference, inter-cell interference, and intra-cell interference are all included in $\bar{\boldsymbol{G}}[n]$. We can write the received signal as

$$\boldsymbol{Y} = \tilde{\boldsymbol{g}}[n]d[n] + \bar{\boldsymbol{G}}[n]\bar{\boldsymbol{A}}[n] + \boldsymbol{V}[n] \tag{4.42}$$

From a geometrical point of view, the columns of $\bar{\boldsymbol{G}}[n]$ span a certain subspace, the *interference subspace*. $\mathcal{S} = \text{span}(\bar{\boldsymbol{G}}[n])$, where span$(\cdot)$ generates all possible linear combinations of the vectors inside the brackets. We

define the projection matrix:

$$\boldsymbol{P}_{\bar{\boldsymbol{G}}[n]} = \bar{\boldsymbol{G}}[n](\bar{\boldsymbol{G}}^H[n]\bar{\boldsymbol{G}}[n])^{-1}\bar{\boldsymbol{G}}^H[n] \tag{4.43}$$

being the unique orthogonal projection onto $\mathcal{S}$; that is, for any $\boldsymbol{x} \in \mathbb{C}^{\mathcal{D}}$, then $\boldsymbol{P}_{\bar{\boldsymbol{G}}[n]}\boldsymbol{x} \in \mathcal{S}$ and $\|\boldsymbol{x} - \boldsymbol{P}_{\bar{\boldsymbol{G}}[n]}\boldsymbol{x}\|^2$ is minimal. $\mathcal{D}$ is the dimension of the vector $\boldsymbol{x}$. Further, we define

$$\boldsymbol{P}^{\perp}_{\bar{\boldsymbol{G}}[n]} = \mathbf{I} - \boldsymbol{P}_{\bar{\boldsymbol{G}}[n]} = \mathbf{I} - \bar{\boldsymbol{G}}[n](\bar{\boldsymbol{G}}^H[n]\bar{\boldsymbol{G}}[n])^{-1}\bar{\boldsymbol{G}}[n]^H \tag{4.44}$$

which is the projection matrix on $\mathcal{S}^{\perp}$ (the orthogonal complement of $\mathcal{S}$), so that for any $\boldsymbol{x} \in \mathbb{C}^{\mathcal{D}}$, then $\boldsymbol{P}^{\perp}_{\bar{\boldsymbol{G}}[n]}\boldsymbol{x} \in \mathcal{S}^{\perp}$.

As the vector obtained in this way has no components in the interference subspace, a simple matched filter ($\tilde{\boldsymbol{g}}^H[n]$) suffices to retrieve the transmitted symbol $d[n]$. Up to a proper scalar scaling factor, the result obtained may be shown to be equivalent to the result obtained by a symbol-level MMSE-ZF equalizer:

$$\hat{d}[n] = \frac{1}{\tilde{\boldsymbol{g}}^H[n]\boldsymbol{P}^{\perp}_{\bar{\boldsymbol{G}}[n]}\tilde{\boldsymbol{g}}[n]}\tilde{\boldsymbol{g}}^H[n]\boldsymbol{P}^{\perp}_{\bar{\boldsymbol{G}}[n]}\boldsymbol{Y} \tag{4.45}$$

while the classical expression for the MMSE-ZF filter would be

$$\hat{a}^{ZF}[n] = \boldsymbol{e}_n^T(\tilde{\boldsymbol{G}}^H[n]\tilde{\boldsymbol{G}}[n])^{-1}\tilde{\boldsymbol{G}}^H[n]\,\mathbf{Y} \tag{4.46}$$

where $\boldsymbol{e}_n$ is a unit vector.

Notice that both the symbol-level MMSE-ZF receiver and the projection receiver need the matrix $\tilde{\boldsymbol{G}}[n]$ (or $\bar{\boldsymbol{G}}$) to be *tall* to have enough degrees of freedom for the inversion. In general, if the number of interferers is not too large (intra-cell codes as well as inter-cell interfernce), the model in Equation (4.41) allows leveraging on the stacking factor (increasing M) to arbitrarily increase the number of rows in the matrix.

4.5.3.1.1 Successive Projection Algorithms

Most of the computational complexity of the projection receiver lies in the inversion of the Grammian term $\bar{\boldsymbol{G}}^H[n]\bar{\boldsymbol{G}}[n]$, which is a square matrix whose dimension is equal to the total number of interfering columns, J.

To avoid performing the inverse, one simplification can be represented by the idea of projecting the received signal successively on each one of the columns that compose $\bar{\boldsymbol{G}}[n]$, $\bar{\boldsymbol{g}}_1[n]$, until $\bar{\boldsymbol{g}}_J[n]$. Doing it vector by vector, the Grammian terms result in a scalar (the squared norm of the considered vector) and the inversion becomes simply a division by a scalar.

The resulting iterative algorithm is the following:

$$\begin{aligned}
&\boldsymbol{Y}^{(0)} = \boldsymbol{Y}[n] \\
&\text{for } i = 1 : J \rightarrow \boldsymbol{Y}^{(i)} = \boldsymbol{Y}^{(i-1)} - \frac{1}{\|\bar{\boldsymbol{g}}_i[n]\|^2}\bar{\boldsymbol{g}}_i[n]\bar{\boldsymbol{g}}_i^H[n]\boldsymbol{Y}^{(i-1)} \\
&\hat{a}_n = \tilde{\boldsymbol{g}}^H[n]\boldsymbol{Y}^{(J)}
\end{aligned} \tag{4.47}$$

This algorithm allows a considerable reduction in complexity compared to the full matrix projection. However, projecting vector by vector separately like this is an *approximation* of the full matrix projection exposed above. The two methods would be equivalent *if and only if* the columns $\tilde{\boldsymbol{g}}_i[n]$ were *orthogonal*. This condition can be achieved by applying a prior orthonormalization process onto the considered vectors, via the Gram–Schmidt procedure or an equivalent one. The one implemented here is a modified version of the Gram–Schmidt procedure, in which the computation of square roots is avoided (square roots have a consistent computational complexity). In fact, for our purposes, the normalization of the basis is not needed. In this way a matrix $\mathbf{U}$ is computed, whose columns form an orthogonal basis for the interference subspace $\mathcal{S}$, and it is on these vectors that the projections are done. The orthogonalization process is provided as follows:

$$\begin{aligned}
&\boldsymbol{u}_1 = \bar{\boldsymbol{g}}_1[n] \\
&\text{for } i = 2 : J \rightarrow \boldsymbol{u}_i = \bar{\boldsymbol{g}}_i[n] - \sum_{k=1}^{i-1} c_{k,i}\boldsymbol{u}_i \\
&\text{where } c_{k,i} = \langle \boldsymbol{u}_k, \bar{\boldsymbol{g}}_i[n] \rangle)
\end{aligned} \tag{4.48}$$

If one basis vector $\boldsymbol{u}_i$ is too small (norm lower than a certain value ε), it is discarded. This means that the rank of the interference matrix $\bar{\boldsymbol{G}}[n]$ is lower than J. Once all the vectors of the basis have been computed, the projection is done on these vectors exactly as in the previous case (Equation (4.47)).

The orthogonalization process allows one to have an *exact* projection algorithm even if performed vector by vector. However, it introduces an additional complexity compared to the direct projection on the columns $\bar{\boldsymbol{G}}[n]$. So both approaches are reasonable, depending on which trade-off between performances and complexity one wants to achieve. The loss in performance deriving from the first approach depends mainly on two factors:

1. How *sparse* the matrix $\bar{\boldsymbol{G}}[n]$ is
2. How *tall* the matrix $\bar{\boldsymbol{G}}[n]$ is

In fact, the more the matrix tends to have such characteristics, the more the inner product between pairs of its columns tends to be small and therefore the condition of orthogonality is approached. Often in practical cases this situation is verified (small number of codes and small number of interfering base stations to cancel) and thus there is no particular need for a prior orthogonalization process because the gap in performance is not enormous.

4.5.3.1.2 Projections on Reduced Subspaces

To reduce the complexity further, one can exploit the fact that not all the interfering vectors $bm\bar{\boldsymbol{g}}_i[n]$ contribute in an equal way to the interference. So the number of vectors to consider can be reduced from the full number J down to a certain subset of *strongest* interferers.

One criterion for the selection of these vectors can be represented by their *inner product* with the column $\tilde{\boldsymbol{g}}[n]$; in this case, we fix a certain threshold ϑ. If the inner product between the columns $\bar{\boldsymbol{g}}_i[n]$ and $\tilde{\boldsymbol{g}}[n]$ is greater than ϑ, the columns will be included in the projection subset, otherwise it will be discarded. The proposed algorithm behaves as follows:

$$
\begin{aligned}
&\boldsymbol{Y}^{(0)} = \mathrm{Y}[n] \\
&\text{for } i = 1 : J \\
&\quad \text{if } \langle \bar{\boldsymbol{g}}_i[n], \tilde{\boldsymbol{g}}[n] \rangle \geq \vartheta \rightarrow \boldsymbol{Y}^{(i)} = \boldsymbol{Y}^{(i-1)} - \frac{1}{\|\bar{\boldsymbol{g}}_i[n]\|^2} \bar{\boldsymbol{g}}_i[n] \bar{\boldsymbol{g}}_i^H[n] \boldsymbol{Y}^{(i-1)} \\
&\text{end} \\
&\hat{a}_n = \tilde{\boldsymbol{g}}[n]^H \boldsymbol{Y}^{(J)}
\end{aligned}
\tag{4.49}
$$

Simulation results show that a proper choice for ϑ can be around 0.2. Furthermore, if the number of selected columns is not very high on average, it is also possible to make the projection on the whole matrix formed by these vectors, which will give better performances.

4.5.4 LMMSE Receiver

Although complete deconvolution is possible for $\tilde{\boldsymbol{G}}$ with the decorrelator $\tilde{\boldsymbol{F}}_{Dec}$, it amplifies the noise term $\boldsymbol{V}$. A better approach is the LMMSE estimator, which models $\boldsymbol{A}$ as a random Gaussian vector and solves the cost criterion

$$
\tilde{\boldsymbol{F}}_{LMMSE} = \arg_{\tilde{\boldsymbol{F}}} \min_{\boldsymbol{A} \in \mathbb{C}^{MK}} \mathbb{E}(\tilde{\boldsymbol{F}}\boldsymbol{Y} - \boldsymbol{A})(\tilde{\boldsymbol{F}}\boldsymbol{Y} - \boldsymbol{A})^H \tag{4.50}
$$

with the solution

$$\tilde{\boldsymbol{F}}_{LMMSE} = \left(\tilde{\boldsymbol{G}}^H \tilde{\boldsymbol{G}} + \boldsymbol{R}_{VV}\right)^{-1} \tilde{\boldsymbol{G}}^H \tag{4.51}$$

which, different from the decorrelator, requires also the noise covariance matrix symbol amplitudes $\boldsymbol{R}_{VV}$. Note that for vanishing noise, $\tilde{\boldsymbol{F}}_{LMMSE}$ becomes equivalent to the decorrelator. For high noise, on the other hand, it is identical to the single-user matched filter (SUMF).

The equivalent model in terms of linear systems of equations can be written as

$$\underbrace{(\boldsymbol{R} + \boldsymbol{R}_{VV})}_{\boldsymbol{T}} \hat{\boldsymbol{A}}_{LMMSE} = \boldsymbol{X} \tag{4.52}$$

where $\boldsymbol{T}$ denotes the SUMF bank output covariance matrix. Both decorrelator and LMMSE receiver are very complex due to the fact they require matrix-inversion operations with $O(M^3K^3)$ complexity. Therefore, reduced rank approximations of the matrix inversion operation have been investigated in the literature with iterative techniques. We elaborate on only the so-called parallel interference cancellation (PIC) family, which is the counterpart of Jacobi iterations for the iterative solutions of linear systems of equations because it works particularly well when user symbols have similar power levels, which is the case for HSDPA. For other state-of-the-art iterative techniques that are not discussed here, such as successive interference cancellation (SIC), which is the counterpart of Gauss–Seidel iterations in matrix algebra or the decorrelating decision feedback equalizer (DFE), see [43] and [11].

4.5.5 Linear Parallel Interference Cancellation (LPIC) Receiver

Conventional LPIC corresponds to using Jacobi iterations for the solutions of linear systems of equations [40]. Splitting the $\boldsymbol{R}$ expression in Equation (4.40) into the two parts as $\boldsymbol{I}$ and $(\boldsymbol{R} - \boldsymbol{I})$, one can obtain the iterative decorrelation solution as[16]

$$\hat{\boldsymbol{A}}_{LS}^{(i)} = (\boldsymbol{I} - \boldsymbol{R})\hat{\boldsymbol{A}}_{LS}^{(i-1)} + \boldsymbol{X} \tag{4.53}$$

The iterations converge provided that the spectral radius $\rho(\boldsymbol{I} - \boldsymbol{R})$ is less than 2, which is not guaranteed.[17]

[16] Similarly splitting $\boldsymbol{T}$ in Equation (4.52) for the LMMSE receiver.

[17] $\rho(\boldsymbol{X}) = \max\{|\lambda|, \lambda \in \Lambda(\boldsymbol{X})\}$, where $\Lambda(\boldsymbol{X})$ is the eigenvalue matrix of $\boldsymbol{X}$.

A better approach is to tackle the problem from the Cayley–Hamilton theorem, which states that every square matrix satisfies its characteristic equation. This principle can be used to find the inverse of an $n \times n$ square matrix by a polynomial expansion as [9]

$$\begin{aligned} det(\boldsymbol{R} - \lambda \boldsymbol{I}) &= 0 \\ &\Rightarrow 1 - c_1\lambda - \cdots - c_{n-1}\lambda^{n-1} - c_n\lambda^n = 0 \\ &\Rightarrow \boldsymbol{I} - c_1\boldsymbol{R} \cdots - c_{n-1}\boldsymbol{R}^{n-1} - c_n\boldsymbol{R}^n = \boldsymbol{0} \\ &\Rightarrow \boldsymbol{I} = c_1\boldsymbol{R} + \cdots + c_{n-1}\boldsymbol{R}^{n-1} + c_n\boldsymbol{R}^n \\ &\Rightarrow \boldsymbol{R}^{-1} = c_1\boldsymbol{I} \cdots + c_{n-1}\boldsymbol{R}^{n-2} + c_n\boldsymbol{R}^{n-1} \end{aligned}$$

With polynomial expansion it is possible to obtain the decorrelator solution or the LMMSE solution in n iterations. Suboptimal solutions are obtained by stopping at a few iterations, in which case the optimal weights change as well. Although this looks like an attractive solution at first sight, the complexity depends on the weight adaptation. See [26] and [27] for two adaptation schemes, one from the direct derivation from the MMSE expression for a particular number of iterations and one from large system analysis. In this text we are not concerned with weight adaptation, but instead with filter adaptation.

4.5.6 Iterative Receivers Based on Chip Equalizers

The LMMSE chip equalizer-correlator receiver does not exploit subspaces in partially loaded systems. This is in contrast to the symbol-level LMMSE receiver, which as discussed below is time-varying due to the scrambler and hence too complex to implement. A compromise can be found by performing symbol-level multi-stage Wiener filtering (MSWF), which is an iterative solution in which the complexity per iteration becomes comparable to twice that of the RAKE receiver. Because MSWF works best when the input is white, better performance is obtained if the RAKE in each MSWF stage is replaced by a chip equalizer-correlator. One of the main contributions here is to point out that the chip equalizer benefits from a separate optimization in every stage. This is shown through a mix of analysis and simulation results.

The LMMSE receiver is complex for UMTS FDD mobile terminals because it not only requires inversion of a large user cross-correlation matrix, but also needs the code and the amplitude knowledge of all the active users [24]. Furthermore, the LMMSE solution changes every chip period due to aperiodic scrambling. The LMMSE *chip* equalizer-correlator is

a suboptimal but much simpler alternative that is derived by modeling the scrambler as a stationary random sequence [20,21]. Another suboptimal multi-user detector that *explicitly* focuses on subtracting the signals of interfering codes is the PIC receiver [43]. It is well known that under very relaxed cell loads, when the number of iterations goes to infinity, PIC might converge to the decorrelating receiver [22]. However, provided that it converges, the convergence rate is still very slow and it requires many stages to obtain a reasonable performance. This is due to the existence of high cross-correlations among users, which in fact is a consequence of the low orthogonality factor obtained initially from the use of a RAKE receiver in the front-end [7,25,29]. In this text, to at least guarantee the convergence in realistic loading factor situations and to increase the speed of convergence, we start the decorrelation operation, that is, the ZF *symbol* equalization from the output of LMMSE chip equalizer-correlator front end receiver whose orthogonality factor is higher than the RAKE receiver. For approximating this matrix inversion operation, we consider the polynomial expansion (PE) technique, which is a better structured equivalent of PIC [26]. Until recently, interference cancellation was considered somewhat reluctantly for the downlink because it unrealistically requires knowing the locations of active codes in the OVSF tree and the amounts of power they carry. Only recently have the merits of inter-cell interference cancellation been acknowledged [5], and efforts at finding viable solutions have more than doubled. The problem of OVSF code indentification can be simplified by an equivalent modeling of the active multi-rate transmission system as a multi-code pseudo-transmission system at any chosen single SF-level L in the OVSF hierarchy. One toy example representing actually the UMTS-TDD case that contains SFs ranging from 1 to 16 is given in Figure 4.21. In this example, the nodes corresponding to the active codes at SF-levels 4 and 8 are demonstrated by black bulbs. Their pseudo-equivalents at SF-level 16 (i.e., $L = 16$) are demonstrated by hatched pattern bulbs.

One can detect the existence or absence of pseudo-codes at the pseudo-level by comparing the powers at their correlator outputs with a noise-floor threshold [23]. These multiple correlations can be implemented with $O(L\,log L)$ complexity using fast Walsh-Hadamard transformation (FWHT). Unitary FWHTs (U-FWHT) with proper dimensions can be logically/physically exploited to see/implement the two-way transformations between actual symbol sequences corresponding to the known codes (e.g., HSDPA codes) at various SF-levels and their pseudo-symbol sequence equivalents at a single SF-level. Figure 4.22 demonstrates the two-way transformations between L_2/L_1 consecutive (time-multiplexed) actual symbols a_i at level L_1 and L_2/L_1 parallel (code-multiplexed) pseudo-symbols $\tilde{a}_i$ at a larger SF-level L_2. $P_{\{L_2/L_1\}}/S$ and $S/P_{\{L_2/L_1\}}$ are parallel to serial and serial to parallel converters from/to a bus size L_2/L_1. When actual symbols reside at a higher SF-level, the two transformations have reverse roles.

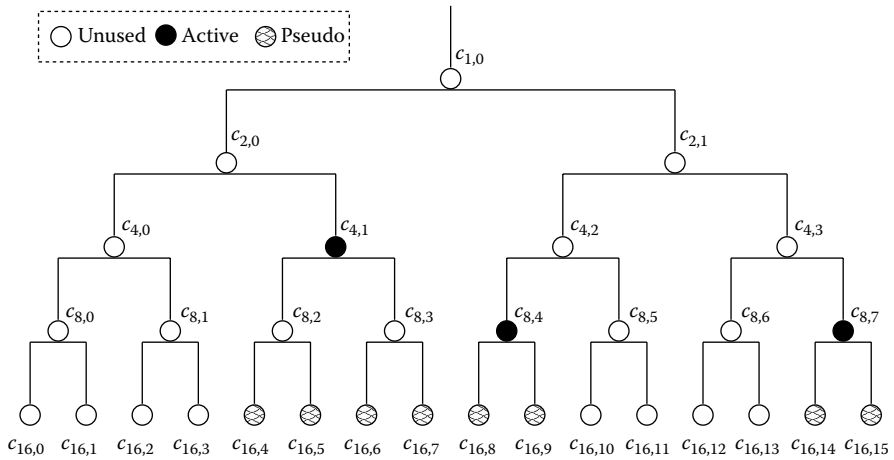

Figure 4.21 Equivalence of active-multirate and pseudo-multicode systems.

4.5.6.1 Polynomial Expansion Receiver

In this section we develop parallel intra-cell interference cancelling (IC) structures based on the polynomial expansion (PE) technique initially proposed in [26]. We exploit the *pseudo-equivalency* concept at the highest *active* SF-level (SF-256), in the UMTS-FDD downlink for applying PE at this level. We ignore the existence of SF-512 because it is rarely used to carry out control commands during an upload operation. The rationale for choosing the *highest active SF*, henceforth called L, is to obtain the highest possible degrees of freedom in determining the PE subspace. If any other level L_x were selected, then an activity on a child code of $c_{x,i}$, $i \in \{0, \ldots, L_x - 1\}$, say, at a level $L_y > L_x$ on $c_{y,j}$, $j \in \{(L_y/L_x)i, \ldots, (L_y/L_x)(i+1) - 1\}$, would also render mandatory the implicit inclusion of all other child codes of $c_{x,i}$ at level L_y by including $c_{x,i}$ in the PE. This would have an adverse effect of noise amplification.

Pseudo-codes might be used in place of the *unknown actual codes* because the actual symbol estimates and their powers are not necessary as

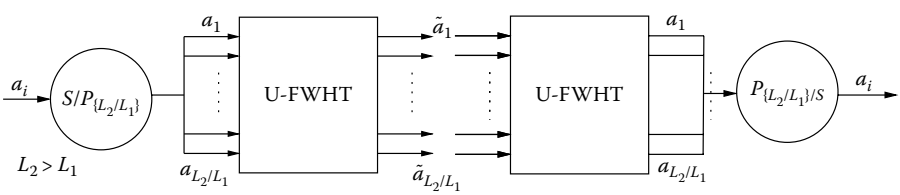

Figure 4.22 Transformations between actual and pseudo-symbols.

long as the pseudo-symbols are treated linearly in interference cancellation. However, knowing or detecting the actual codes is an opportunity for exploiting hard or hyperbolic-tangent nonlinearities or even channel decoding and encoding to refine their symbol estimates [10,18]. In the latter case, one can pass between the symbol blocks of known codes and their pseudo-equivalents at SF-256 by properly dimensioned FWHTs. Through this hybrid treatment, respective nonlinear and linear treatment of known and unknown codes becomes possible.

We model the discrete time received signal over one pseudo-symbol period as

$$\boldsymbol{Y}[n] = \boldsymbol{H}(z)\boldsymbol{S}[n]\boldsymbol{C}\boldsymbol{A}[n] + \boldsymbol{V}[n] = \widetilde{\boldsymbol{G}}(n, z)\boldsymbol{A}[n] + \boldsymbol{V}[n]$$

representing the system at the symbol rate. As shown in Figure 4.23, $\boldsymbol{H}(z) = \sum_{i=0}^{M-1} \boldsymbol{H}[i]\, z^{-i}$ is the symbol rate $Lm \times L$ channel transfer function, z^{-1} being the symbol period delay operator. The block coefficients $\boldsymbol{H}(i)$ are

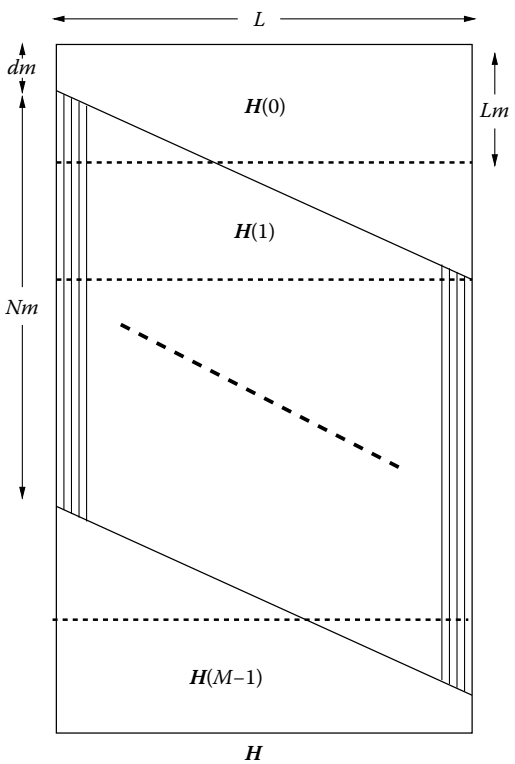

Figure 4.23 Channel impulse response of $\boldsymbol{H}(z)$.

the $M = \lceil \frac{L+N+d-1}{L} \rceil$ parts of the block Toeplitz matrix with $m \times 1$ sized blocks, $\boldsymbol{b}$ being the first column whose top entries might be zero for it comprises the transmission delay d between the BS and the mobile terminal. In this representation, $\boldsymbol{H}[0]$ carries the signal part corresponding to $\boldsymbol{A}[n]$ where there is no user of interest inter-symbol interference (ISI) but only user of interest ICI and MUI. $\boldsymbol{H}(i)$, $(i \in \{1, 2, \ldots, M-1\})$, similarly carries the ICI and MUI from $\boldsymbol{A}[n-i]$. The $L \times L$ matrix $\boldsymbol{S}[n]$ is diagonal and contains the scrambler for symbol period n. The column vector $\boldsymbol{A}[n]$ contains the K (pseudo-)symbols and $\boldsymbol{C}$ is the $L \times K$ matrix of the K active codes.

Although it is possible to find an FIR left inverse filter for $\tilde{\boldsymbol{G}}(n, z)$ provided that $Lm \geq K$, this is not practical because $\tilde{\boldsymbol{G}}(n, z)$ is time-varying due to the aperiodicity of the scrambling. Therefore, we introduce a less complex approximation to this inversion based on the polynomial expansion technique [26]. Instead of basing the receiver directly on the received signal, we first introduce a dimensionality reduction step from Lm to K by equalizing the channels with LMMSE-ZF chip rate equalizers $\boldsymbol{F}(z)$, followed by a bank of correlators. An LMMSE-ZF equalizer is the one among all possible ZF equalizers that minimizes the MSE at its output [14].

Let $\boldsymbol{X}[n]$ be the $K \times 1$ correlator output, which would correspond to the RAKE receiver outputs if channel-matched filters were used instead of channel equalizers. Then,

$$\begin{aligned}\boldsymbol{X}[n] &= \tilde{\boldsymbol{F}}(n, z)\boldsymbol{Y}[n] \\ &= \boldsymbol{C}^H \boldsymbol{S}^H[n]\boldsymbol{F}(z)(\tilde{\boldsymbol{G}}(n, z)\boldsymbol{A}[n] + \boldsymbol{V}[n]) \\ &= \boldsymbol{M}(n, z)\boldsymbol{A}[n] + \tilde{\boldsymbol{F}}(n, z)\boldsymbol{V}[n]\end{aligned}$$

where $\boldsymbol{M}(n, z) = \tilde{\boldsymbol{F}}(n, z)\tilde{\boldsymbol{G}}(n, z)$ and ZF equalization results in $\boldsymbol{F}(z)\boldsymbol{H}(z) = \boldsymbol{I}$. Hence,

$$\boldsymbol{M}(n, z) = \sum_{i=-\infty}^{\infty} \boldsymbol{M}[n, i]z^{-i} = \begin{bmatrix} \boldsymbol{I} & * \\ * & \boldsymbol{I} \end{bmatrix} \tag{4.54}$$

due to proper normalization of the code energies.

To obtain the estimate of $\boldsymbol{A}[n]$, we initially consider the processing of $\boldsymbol{X}[n]$ by a decorrelator as

$$\begin{aligned}\widehat{\boldsymbol{A}}[n] &= \boldsymbol{M}(n, z)^{-1}\boldsymbol{X}[n] \\ &= (\boldsymbol{I} - \overline{\boldsymbol{M}}(n, z))^{-1}\boldsymbol{X}[n]\end{aligned} \tag{4.55}$$

The correlation matrix $\boldsymbol{M}(n, z)$ has a coefficient $\boldsymbol{M}[n, 0]$ with a dominant unit diagonal in the sense that all other elements of the $\boldsymbol{M}[n, i]$ are much

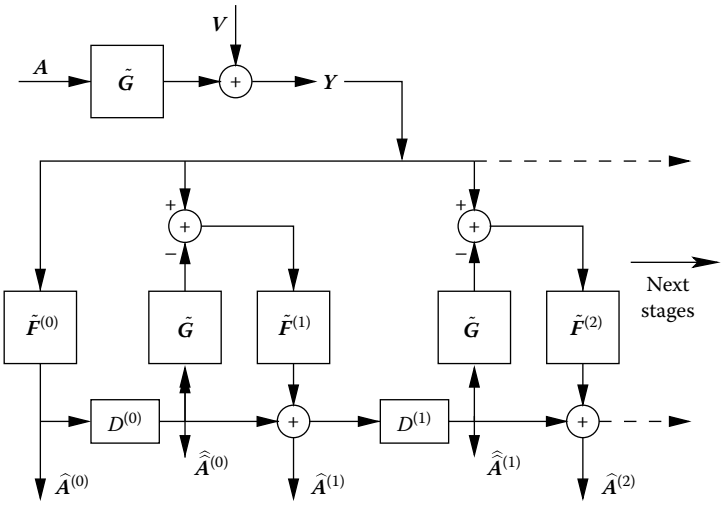

Figure 4.24 Polynomial expansion receiver.

smaller than 1 in magnitude. Hence, the polynomial expansion approach suggests to develop $(\boldsymbol{I} - \overline{\boldsymbol{M}}(n, z))^{-1} = \sum_{i=0}^{\infty} \overline{\boldsymbol{M}}(n, z)^i$ up to some finite order, which leads to the iterative receiver as[18]

$$\begin{aligned}
\widehat{\boldsymbol{A}}^{(-1)} &= 0; \quad i \geq 0 \\
\widehat{\boldsymbol{A}}^{(i)} &= \boldsymbol{X} + \overline{\boldsymbol{M}}\,\widehat{\boldsymbol{A}}^{(i-1)} \\
&= \boldsymbol{X} + (\boldsymbol{I} - \boldsymbol{M})\,\widehat{\boldsymbol{A}}^{(i-1)} \\
&= \widehat{\boldsymbol{A}}^{(i-1)} + \tilde{\boldsymbol{F}}^{i}(\boldsymbol{Y} - \tilde{\boldsymbol{G}}\widehat{\boldsymbol{A}}^{(i-1)})
\end{aligned} \tag{4.56}$$

The resultant iterative receiver architecture is given in Figure 4.24 where the numbers in parantheses indicate the iteration indices. A practical receiver would be limited to a few orders, the quality of which depends on the degree of dominance of the static part of the diagonal of $\boldsymbol{M}(n, z)$ given in Equation (4.56) with respect to the ICI carrying dynamic contents of the diagonal elements and MUI carrying off-diagonal elements.

[18] Time indices are dropped for brevity.

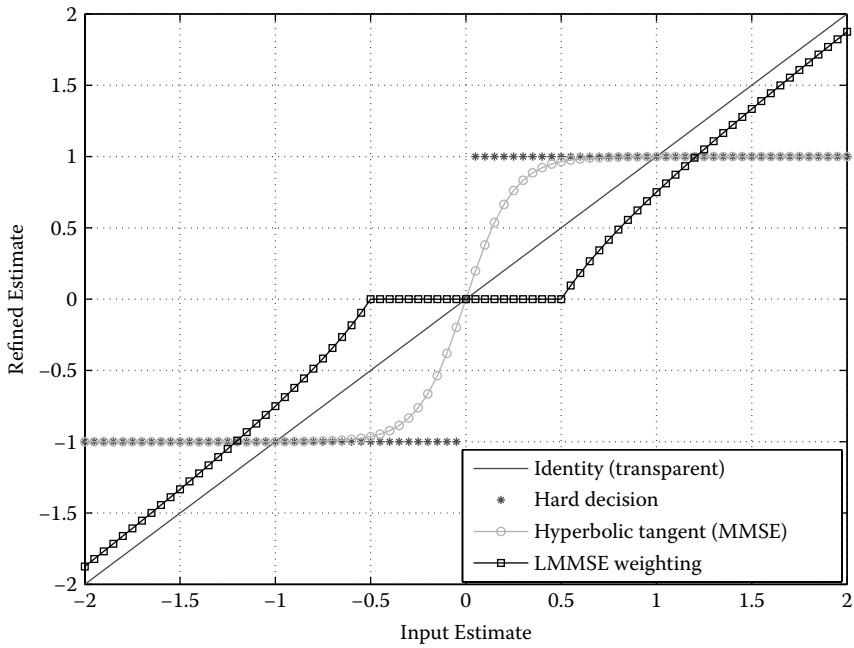

Figure 4.25 Feedback functionalities for real and imaginary parts of QPSK symbols that have 6-dB SINR.

In an iterative PE approach, it is advantageous to replace several *local* receiver components obtained from *global* LMMSE-ZF formulation with their LMMSE counterparts. Such modifications should lead to smaller off-diagonal power and hence faster convergence of the iterations to an estimate that is closer to a global MMSE estimate. For example, LMMSE-ZF chip equalizers can be replaced by LMMSE equalizers that, although perturb the orthogonal structure of the received signal from the BS, do not enhance as much the inter-cell interference plus noise [28]. Furthermore, some symbol feedback functionalities $\mathcal{D}$ shown in Figure 4.25 such as LMMSE weighting factors, hard decisions, a variety of soft decisions like hyperbolic-tangent functionality or even channel decoding and encoding blocks can be introduced.

4.5.6.1.1 Filter Adaptation

Figure 4.26 shows the open form of the receiver in Figure 4.24 where we clearly see the chip-level blocks. In case the symbol feedback functionality $\mathcal{D}$ is the identity matrix, we can further obtain a third equivalent architecture

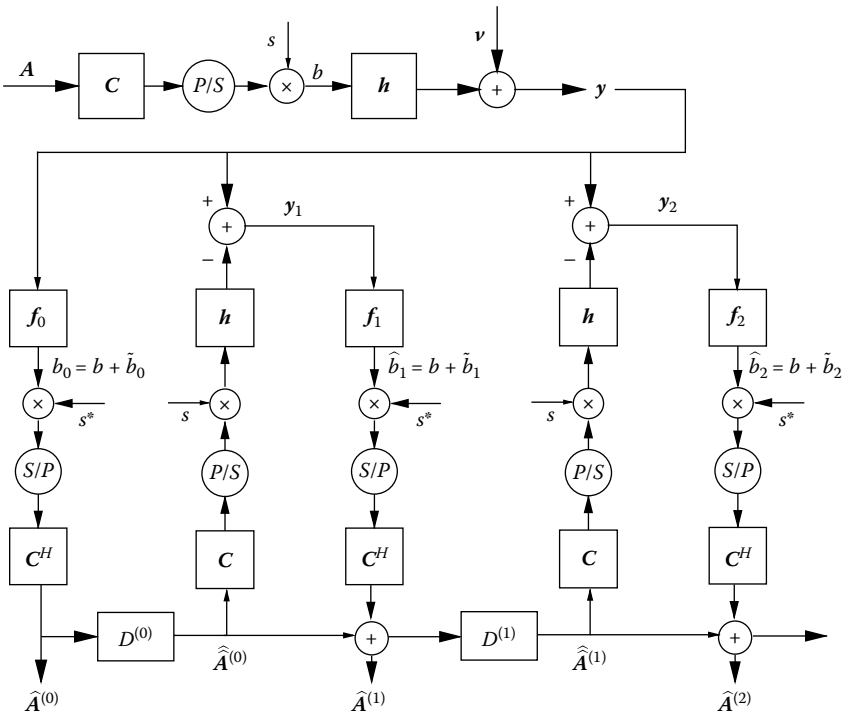

Figure 4.26 Polynomial expansion receiver open format.

given in Figure 4.27 that, different from the previous two, iterates over the *chip* estimates at chip-level filter outputs.

Because the projection operation $\boldsymbol{S}[n]\boldsymbol{C}\boldsymbol{C}^H\boldsymbol{S}^*[n]$ is not a chip-level operation and is not convolutive, it cannot be easily integrated into the filter optimization process. Nevertheless it has two nice properties: (1) the diagonal part is the deterministic value $\mathcal{C}_l\boldsymbol{I}$ where $\mathcal{C}_l$ is the effective cell loading factor and (2) the expected value of the non-diagonal part is zero. By considering only the diagonal parts of the local projection operations, we reach the multi-stage Wiener (LMMSE) filter adaptation procedure given in the Equation group (4.57) where $\{\boldsymbol{\mathcal{X}}_i, \boldsymbol{\mathcal{Y}}_i, \tilde{\boldsymbol{B}}_i\}$, respectively, denote transfer function between the BS signal and the residual BS signal, transfer function for the intercell interference plus noise, the residual interference plus noise at iteration i.[19] The Wiener (LMMSE)

[19] Each bold variable in this section has a (z) suffix, which is dropped for brevity; † stands for z-transform para-conjugate operator meaning matched filter in the time domain.

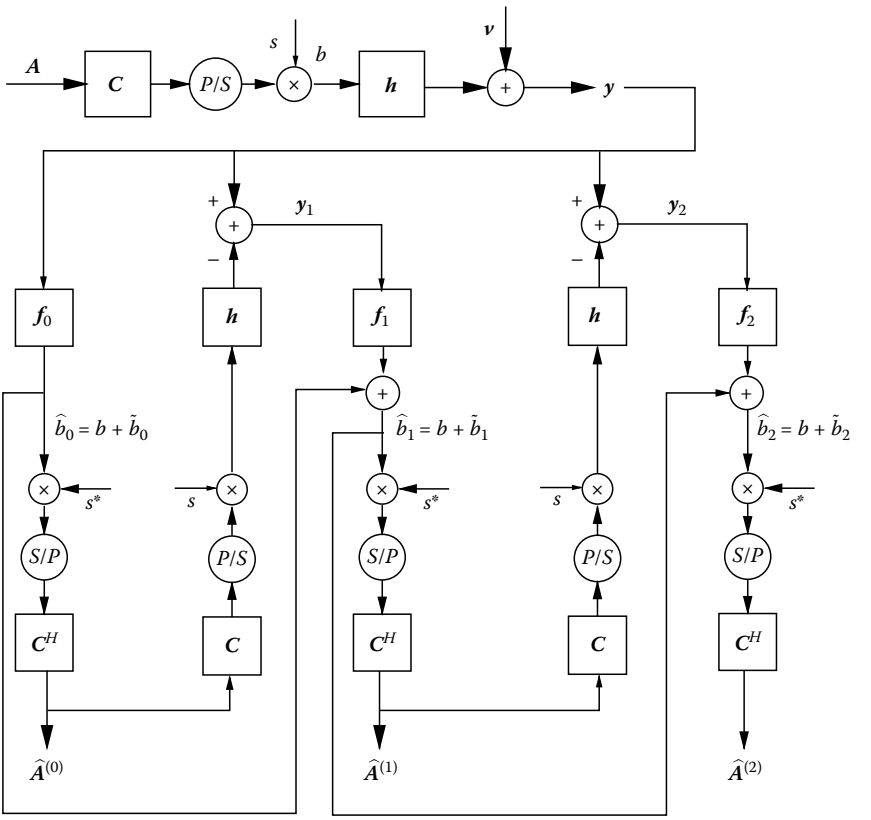

Figure 4.27 PE receiver equivalent chip estimate iterating model.

filter and the unbiased LMMSE filter are denoted by $\boldsymbol{F}_i^w$ and $\boldsymbol{F}_i$, respectively.

The LMMSE optimization process output is the complete filter expression of $\boldsymbol{F}_i$, from which we derive its two ingredients $\boldsymbol{S}_{\tilde{b}_{i-1}\boldsymbol{y}_i}$ and $\boldsymbol{S}_{\boldsymbol{y}_i\boldsymbol{y}_i}$ by *factorization*. The structure of the factorized terms are clear guidelines for understanding that, when unbiased, the chip-level filter $\boldsymbol{F}_i$ intends to estimate and subtract the *residual interference plus noise* term at the preceding iteration, which is expected to be also valid for systems with additional system components such as hard decisions. For example, if we consider the loop among the signals $\hat{b}_0$, $\boldsymbol{y}_1$, and $\hat{b}_1$ that contains the transfer functions $\boldsymbol{F}_1(z)$ and $\boldsymbol{H}(z)$, it estimates the residual signal $\tilde{b}_0$ and subtracts it from $\hat{b}_0$, which leads to the creation of the new residual signal $\tilde{b}_1$. The same reasoning holds for subsequent iterations where the amount of interference plus

noise variance $\sigma^2_{\tilde{b}_i}$ is expected to decrease with increasing i as long as the spectral radius $\rho(\boldsymbol{I} - \mathcal{C}_l \boldsymbol{F}_i \boldsymbol{H}) < 1$.

INITIALIZATION (First Stage)

$$\boldsymbol{\mathcal{X}}_0 = \boldsymbol{F}_0 \boldsymbol{H} - \boldsymbol{I}$$

$$\boldsymbol{\mathcal{Y}}_0 = \boldsymbol{F}_0$$

$$\tilde{\boldsymbol{B}}_0 = \boldsymbol{\mathcal{X}}_0 \boldsymbol{B} + \boldsymbol{\mathcal{Y}}_0 \boldsymbol{V}$$

ITERATIONS (Interference Cancellation Stages)

for ($i > 0$) and ($i < i_{max}$)

$$\boldsymbol{\mathcal{X}}_i = (\boldsymbol{I} - \mathcal{C}_l \boldsymbol{F}_i \boldsymbol{H}) \boldsymbol{\mathcal{X}}_{i-1}$$

$$\boldsymbol{\mathcal{Y}}_i = (\boldsymbol{I} - \mathcal{C}_l \boldsymbol{F}_i \boldsymbol{H}) \boldsymbol{\mathcal{Y}}_{i-1} + \boldsymbol{F}_i$$

$$\tilde{\boldsymbol{B}}_i = \boldsymbol{\mathcal{X}}_i \boldsymbol{B} + \boldsymbol{\mathcal{Y}}_i \boldsymbol{V}$$

$$\arg_{\boldsymbol{F}_i^w} \min \frac{1}{2\pi j} \oint \frac{dz}{z} \left(\boldsymbol{\mathcal{X}}_i \boldsymbol{\mathcal{X}}_i^{\dagger} \sigma_b^2 + \boldsymbol{\mathcal{Y}}_i \boldsymbol{\mathcal{Y}}_i^{\dagger} \sigma_v^2 \right) \tag{4.57}$$

$$\boldsymbol{F}_i^w = \boldsymbol{S}_{\tilde{b}_{i-1} \boldsymbol{y}_i} \boldsymbol{S}^{-1}_{\boldsymbol{y}_i \boldsymbol{y}_i}$$

$$\boldsymbol{S}_{\tilde{b}_{i-1} \boldsymbol{y}_i} = \mathcal{C}_l \boldsymbol{\mathcal{X}}_{i-1} \boldsymbol{\mathcal{X}}_{i-1}^{\dagger} \boldsymbol{H}^{\dagger} \sigma_b^2 - \boldsymbol{\mathcal{Y}}_{i-1} (\boldsymbol{I} - \mathcal{C}_l \boldsymbol{H} \boldsymbol{\mathcal{Y}}_{i-1})^{\dagger} \sigma_v^2$$

$$\boldsymbol{S}_{\boldsymbol{y}_i \boldsymbol{y}_i} = \mathcal{C}_l^2 \boldsymbol{H} \boldsymbol{\mathcal{X}}_{i-1} \boldsymbol{\mathcal{X}}_{i-1}^{\dagger} \boldsymbol{H}^{\dagger} \sigma_b^2 + (\boldsymbol{I} - \mathcal{C}_l \boldsymbol{H} \boldsymbol{\mathcal{Y}}_{i-1})(\boldsymbol{I} - \mathcal{C}_l \boldsymbol{H} \boldsymbol{\mathcal{Y}}_{i-1})^{\dagger} \sigma_v^2$$

$$\boldsymbol{F}_i = \frac{2\pi j \boldsymbol{F}_i^w}{\oint \frac{dz}{z} \boldsymbol{F}_i^w \boldsymbol{H}} : \text{unbiasing operation} \tag{4.58}$$

end

In practice, LMMSE chip equalizer correlator blocks might also be implemented as Generalized RAKE (G-RAKE) receivers in which case, in each stage, filtering with $\boldsymbol{F}_i$ and $\boldsymbol{H}$ will be similar to the filtering part of the RAKE receiver [45]. Hence, each iteration will have twice the complexity of that of the RAKE.

4.5.6.1.2 Impact of Symbol Feedback Nonlinearities on Filter Expressions

When hard decisions or hyperbolic tangent nonlinearities are used on a subset of codes, we see two alternatives to reflect their impact on filtering expressions. The first approach is to simply assume that the associated symbols are perfectly estimated and hence to exclude them after the first stage. In this case, the only required changes are to consider $\mathcal{C}_l$ and σ_b^2 as, respectively, the loading factor and the sum chip variance of the remaining codes that are treated linearly. The second approach is to quantify the

variances of symbol estimation errors after the nonlinearities at every stage by the scheme and introduce new additive Gaussian noise sources at those points with the obtained variances.

4.5.6.2 Intercell Interference Cancellation Expansion

The polynomial expansion receiver can be modified to include also the inter-cell interference cancellation. The filter adaptations, the changes in signal modeling, and the architecture for cancelling the interference of one neighboring BS are given in Equation group (4.59), Equation group (4.60) and Figure 4.28. The scheme can be easily extended to cover any number of cells by increasing the sizes of vectors and matrices in Equation group (4.60).

INITIALIZATION (First Stage)

$$\boldsymbol{\mathcal{X}}_0 = \boldsymbol{F}_0\boldsymbol{H} - \boldsymbol{I}$$

$$\boldsymbol{\mathcal{Y}}_0 = \boldsymbol{F}_0$$

$$\tilde{\boldsymbol{B}}_0 = \boldsymbol{\mathcal{X}}_0\boldsymbol{B} + \boldsymbol{\mathcal{Y}}_0\boldsymbol{V}$$

ITERATIONS (Interference Cancellation Stages)

for $(i > 0)$ and $(i < i_{max})$

$$\boldsymbol{\mathcal{X}}_i = (\boldsymbol{I} - \boldsymbol{F}_i\boldsymbol{H}\boldsymbol{\mathcal{C}}_l)\boldsymbol{\mathcal{X}}_{i-1}$$

$$\boldsymbol{\mathcal{Y}}_i = (\boldsymbol{I} - \boldsymbol{F}_i\boldsymbol{H}\boldsymbol{\mathcal{C}}_l)\boldsymbol{\mathcal{Y}}_{i-1} + \boldsymbol{F}_i$$

$$\tilde{\boldsymbol{B}}_i = \boldsymbol{\mathcal{X}}_i\boldsymbol{B} + \boldsymbol{\mathcal{Y}}_i\boldsymbol{V}$$

$$\arg_{\boldsymbol{F}^w_{1,i}} \min \frac{1}{2\pi j}\oint \frac{dz}{z}\left(\boldsymbol{\mathcal{X}}_{1,i}\boldsymbol{\Sigma}^2_b\boldsymbol{\mathcal{X}}^\dagger_{1,i} + \boldsymbol{\mathcal{Y}}_{1,i}\boldsymbol{\mathcal{Y}}^\dagger_{1,i}\sigma^2_v\right) \tag{4.59}$$

$$\arg_{\boldsymbol{F}^w_{2,i}} \min \frac{1}{2\pi j}\oint \frac{dz}{z}\left(\boldsymbol{\mathcal{X}}_{2,i}\boldsymbol{\Sigma}^2_b\boldsymbol{\mathcal{X}}^\dagger_{2,i} + \boldsymbol{\mathcal{Y}}_{2,i}\boldsymbol{\mathcal{Y}}^\dagger_{2,i}\sigma^2_v\right)$$

$$\boldsymbol{F}^w_{1,i} = \boldsymbol{S}_{\tilde{b}_{1,i-1}\boldsymbol{y}_i}\boldsymbol{S}^{-1}_{\boldsymbol{y}_i\boldsymbol{y}_i} \qquad \boldsymbol{F}^w_{2,i} = \boldsymbol{S}_{\tilde{b}_{2,i-1}\boldsymbol{y}_i}\boldsymbol{S}^{-1}_{\boldsymbol{y}_i\boldsymbol{y}_i}$$

$$\boldsymbol{S}_{\tilde{b}_{1,i-1}\boldsymbol{y}_i} = \mathcal{C}_{l_1}\boldsymbol{\mathcal{X}}_{1,i-1}\boldsymbol{\Sigma}^2_b\boldsymbol{\mathcal{X}}^\dagger_{1,i-1}\boldsymbol{H}^\dagger_1 - \boldsymbol{\mathcal{Y}}_{1,i-1}(\boldsymbol{I} - \mathcal{C}_{l_1}\boldsymbol{H}_1\boldsymbol{\mathcal{Y}}_{1,i-1})^\dagger\sigma^2_v$$

$$\boldsymbol{S}_{\tilde{b}_{2,i-1}\boldsymbol{y}_i} = \mathcal{C}_{l_2}\boldsymbol{\mathcal{X}}_{2,i-1}\boldsymbol{\Sigma}^2_b\boldsymbol{\mathcal{X}}^\dagger_{2,i-1}\boldsymbol{H}^\dagger_2 - \boldsymbol{\mathcal{Y}}_{2,i-1}(\boldsymbol{I} - \mathcal{C}_{l_2}\boldsymbol{H}_2\boldsymbol{\mathcal{Y}}_{2,i-1})^\dagger\sigma^2_v$$

$$\boldsymbol{S}_{\boldsymbol{y}_i\boldsymbol{y}_i} = \boldsymbol{H}\boldsymbol{\mathcal{C}}_l\boldsymbol{\mathcal{X}}_{i-1}\boldsymbol{\Sigma}^2_b\boldsymbol{\mathcal{X}}^\dagger_{i-1}\boldsymbol{\mathcal{C}}_l\boldsymbol{H}^\dagger + (\boldsymbol{I} - \boldsymbol{H}\boldsymbol{\mathcal{C}}_l\boldsymbol{\mathcal{Y}}_{i-1})(\boldsymbol{I} - \boldsymbol{H}\boldsymbol{\mathcal{C}}_l\boldsymbol{\mathcal{Y}}_{i-1})^\dagger\sigma^2_v$$

$$\boldsymbol{F}_{1,i} = \frac{2\pi j\boldsymbol{F}^w_{1,i}}{\oint \frac{dz}{z}\boldsymbol{F}^w_{1,i}\boldsymbol{H}_1} \qquad \boldsymbol{F}_{2,i} = \frac{2\pi j\boldsymbol{F}^w_{2,i}}{\oint \frac{dz}{z}\boldsymbol{F}^w_{2,i}\boldsymbol{H}_2}$$

end

$$
\begin{aligned}
\boldsymbol{A}[n] &\longrightarrow \begin{bmatrix}\boldsymbol{A}_1[n]\\ \boldsymbol{A}_2[n]\end{bmatrix} : \text{vector of symbols}\\
\boldsymbol{C} &\longrightarrow \begin{bmatrix}\boldsymbol{C}_1 & \boldsymbol{0}\\ \boldsymbol{0} & \boldsymbol{C}_2\end{bmatrix} : \text{channelization codes}\\
\boldsymbol{S}[n] &\longrightarrow \begin{bmatrix}\boldsymbol{S}_1[n] & \boldsymbol{0}\\ \boldsymbol{0} & \boldsymbol{S}_2[n]\end{bmatrix} : \text{scrambling}\\
\boldsymbol{B} &\longrightarrow \begin{bmatrix}\boldsymbol{B}_1\\ \boldsymbol{B}_2\end{bmatrix} : \text{transmitted chip sequences}\\
\sigma_b^2 &\longrightarrow \boldsymbol{\Sigma}_b^2 = \begin{bmatrix}\sigma_{b_1}^2 & 0\\ 0 & \sigma_{b_2}^2\end{bmatrix} : \text{chip-level signal covariance}\\
\boldsymbol{H}(z) &\longrightarrow \begin{bmatrix}\boldsymbol{H}_1(z) & \boldsymbol{H}_2(z)\end{bmatrix} : \text{chip rate channel}\\
\boldsymbol{F}_i(z) &\longrightarrow \begin{bmatrix}\boldsymbol{F}_{1,i}(z)\\ \boldsymbol{F}_{2,i}(z)\end{bmatrix} : \text{chip-level equalizers at iteration } i\\
\tilde{\boldsymbol{G}}(n,z) &\longrightarrow \begin{bmatrix}\tilde{\boldsymbol{G}}_1(n,z) & \tilde{\boldsymbol{G}}_2(n,z)\end{bmatrix} = \begin{bmatrix}\boldsymbol{H}_1(z)\boldsymbol{S}_1[n]\boldsymbol{C}_1 & \boldsymbol{H}_2(z)\boldsymbol{S}_2[n]\boldsymbol{C}_2\end{bmatrix}:\\
&\quad \text{symbol rate channel}\\
\tilde{\boldsymbol{F}}^{(i)}(n,z) &\longrightarrow \begin{bmatrix}\tilde{\boldsymbol{F}}_1^{(i)}(n,z)\\ \tilde{\boldsymbol{F}}_2^{(i)}(n,z)\end{bmatrix} : \text{symbol-level equalizers at iteration } i\\
\boldsymbol{\mathcal{X}}_i &\longrightarrow \begin{bmatrix}\boldsymbol{\mathcal{X}}_{1,1,i} & \boldsymbol{\mathcal{X}}_{1,2,i}\\ \boldsymbol{\mathcal{X}}_{2,1,i} & \boldsymbol{\mathcal{X}}_{2,2,i}\end{bmatrix} : \text{interference transfer function}\\
\boldsymbol{\mathcal{X}}_{1,i} &= \begin{bmatrix}\boldsymbol{\mathcal{X}}_{1,1,i} & \boldsymbol{\mathcal{X}}_{1,2,i}\end{bmatrix} : \text{interference transfer function for the first}\\
&\quad \text{BS signal}\\
\boldsymbol{\mathcal{X}}_{2,i} &= \begin{bmatrix}\boldsymbol{\mathcal{X}}_{2,1,i} & \boldsymbol{\mathcal{X}}_{2,2,i}\end{bmatrix} : \text{interference transfer function for the second}\\
&\quad \text{BS signal}\\
\boldsymbol{\mathcal{Y}}_i &\longrightarrow \begin{bmatrix}\boldsymbol{\mathcal{Y}}_{1,i}\\ \boldsymbol{\mathcal{Y}}_{2,i}\end{bmatrix} : \text{noise transfer function}\\
\mathcal{C}_l &\longrightarrow \boldsymbol{\mathcal{C}}_l = \begin{bmatrix}\mathcal{C}_{l_1} & 0\\ 0 & \mathcal{C}_{l_2}\end{bmatrix} : \text{loading factors}\\
\boldsymbol{Y}[n] &\longrightarrow \begin{bmatrix}\boldsymbol{H}_1(z)\boldsymbol{S}_1[n]\boldsymbol{C}_1 & \boldsymbol{H}_2(z)\boldsymbol{S}_2[n]\boldsymbol{C}_2\end{bmatrix}\begin{bmatrix}\boldsymbol{A}_1[n]\\ \boldsymbol{A}_2[n]\end{bmatrix} + \boldsymbol{V}[n]\\
&= \tilde{\boldsymbol{G}}(n,z)\,\boldsymbol{A}[n] + \boldsymbol{V}[n]
\end{aligned}
\tag{4.60}
$$

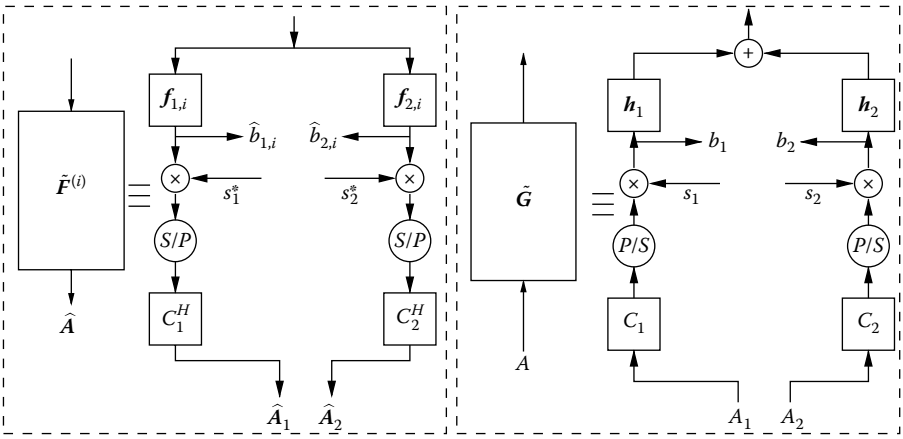

Figure 4.28 Symbol-level transfer function blocks and their chip-level equivalents.

4.5.6.3 Simulations and Conclusions

For the simulations, we consider only intra-cell interference cancellation.

We take a High-Speed Downlink Packet Access (HSDPA) scenario in the UMTS-FDD downlink [5]. We consider five HSDPA codes at SF-16 assigned to the UE, each consuming 8% of the base station power. The PCPICH pilot tone at SF-256 consumes 10% power. There is the PCCPCH code at SF-256 that consumes 4% power. To effectively model all remaining multirate user codes that we do not know, we place 46 pseudo-codes at level 256, each having 1% power. So in total, five HSDSCH codes at SF-16 being equivalent to 80 pseudo-codes at SF-256, the system is effectively 50% loaded with 128 (pseudo-)codes at SF-256; that is, $\mathcal{C}_l = 0.5$. Although, in practice, the pseudo-codes should be detected by a method explained in the text, for the moment we assume that they are known. We also assume perfect knowledge of the channel. An oversampling factor of 2 and one receive antenna are used.[20] Static propagation channel parameters are randomly generated from the ITU Vehicular-A power delay profile. Pulse shape is the UMTS-standard, root-raised cosine with a roll-off factor of 0.22. Therefore, the propagation channel, pulse shape cascade (i.e., the overall channel) has a length of 19 chips at a 3.84 Mchips/s transmission rate. Symbols are QPSK. $\hat{I}_{or}/I_{oc}$ denotes the received base station power to inter-cell interference plus noise power ratio. We took the average SINR result of five HSDPA codes over 100 realizations of one UMTS slot (160 symbol period) transmissions.

[20] The order of filtering and rechanneling operations have an impact on the noise term in case of polyphase filtering, which we neglect for the moment.

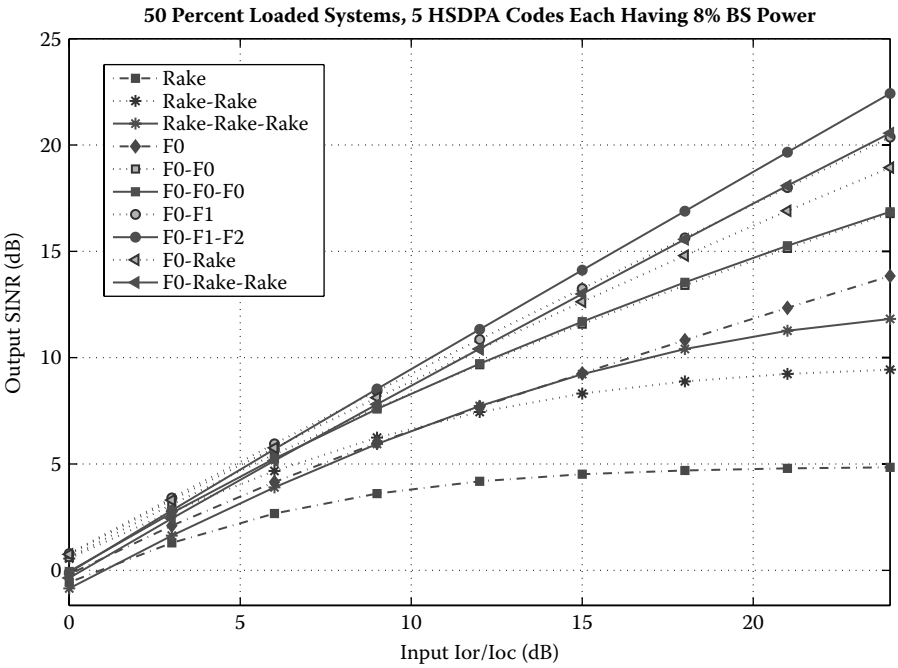

Figure 4.29 SINR versus $\hat{I}_{or}/I_{oc}$ linear decisions results, Vehicular A channel, $N = 19$. 50% loaded systems; 5 HSDPA codes, each having 8% BS power.

Figure 4.29 shows the performances of the PE scheme with various chip-level filter usages and iterations from one to three. The legends indicate the used filters with iteration order. For example, F0-F1-F2 means optimized filters are used in all stages; the F0-Rake-Rake hybrid scheme means the first stage filter is an LMMSE chip equalizer and the subsequent two are Rake receivers; Rake-Rake-Rake corresponds to the *conventional* linear PIC. Many other variants different from the ones shown can also be used. As expected, the RAKE receiver performs the worst. The conventional linear PIC with only RAKE receivers starts diverging after the first iteration, especially for $\hat{I}_{or}/I_{oc}$ values below 10 dB. This is consistent with the literature because it is well known that, for guaranteeing the convergence of the LPIC, the loading factor should be lower than 17% [15].[21] The scheme that uses only F0 does not improve significantly after the second iteration. Using RAKE receivers after F0 performs very well. As expected, adapting the filters at all

[21] In the random CDMA, flat fading case.

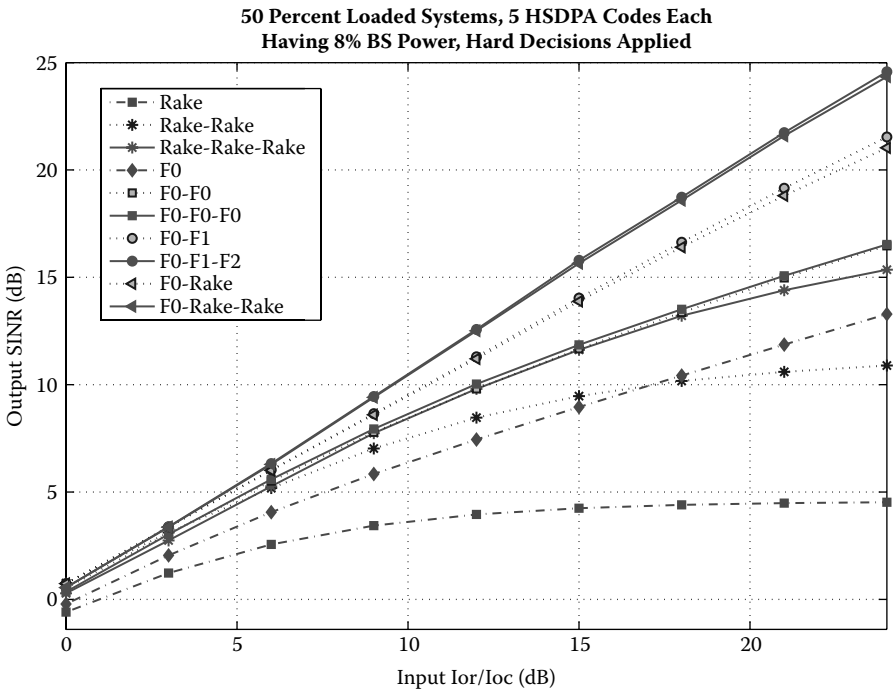

Figure 4.30 SINR versus $\hat{I}_{or}/I_{oc}$ hard decisions results, Vehicular A channel, $N = 19$. 50% loaded systems; 5 HSDPA codes, each having 8% BS power; hard decision applied.

iterations performs the best. Such a scheme obtains almost the same performance as F0-Rake-Rake in one less iteration, that is, with configuration F0-F1. At low $\hat{I}_{or}/I_{oc}$ values, which reflect the cell-edge situations, the performance of the first iteration is better than the second one. This is due to the fact that in low SNR regions, the gain from the interference reduction is not sufficient to compensate for the loss from noise amplification, because the iterative scheme is still a decorrelation. One might also attribute this to the well-known *ping-pong* effect for LPIC [33].

Figure 4.30 shows the performances when we apply hard decisions on the five HSDPA codes, which have an effective loading impact $\mathcal{C}_{HSDPA} = \frac{5}{16}$. With the assumption of correct decisions we subtract $\mathcal{C}_{HSDPA}$ from the overall cell load of 0.5 and apply the $\mathcal{C}_I = \frac{3}{16}$ value in the filter adaptation process in Equation (4.58). In this case, using RAKE receivers after first-stage equalization catches up with the optimized filters after three stages. We also observe that conventional PIC also starts getting into a convergence trend.

It is not, however, explicit from the $\mathcal{X}_i$ and $\mathcal{Y}_i$ expressions why things should improve despite the fact that the $\mathcal{C}_I$ value decreases, resulting in lower iteration gain in chip estimation. Due to this fact, one would at first sight expect an inability of the interference reduction to compensate for the amplified noise. This is, however, not the case, because almost all ingredients of the additional noise term coming from the previous iteration are in the subspace belonging to the codes whose symbols are estimated linearly, whereas the final SINR performance metric is computed on codes such as HSDPA codes, which are treated by hard decisions. In the full linear treatment, however, the additional noise that traverses the iterations with amplification is in the whole signal space. Therefore, when hard decisions are applied, there is an implicit reduction in additional noise by a factor $\frac{\mathcal{C}_I}{\mathcal{C}_I+\mathcal{C}_{HSDPA}}$. These interpretations seem to be in conflict with the chip equalizer adaptation expressions where we ignored the non-diagonal part of the projection operation $\boldsymbol{S}[n]\boldsymbol{C}\boldsymbol{C}^H\boldsymbol{S}^*[n]$ in order to avoid considering dependence on codes. For the interpretations of performances at symbol levels, however, one must look from a different perspective, taking into account the code knowledge.

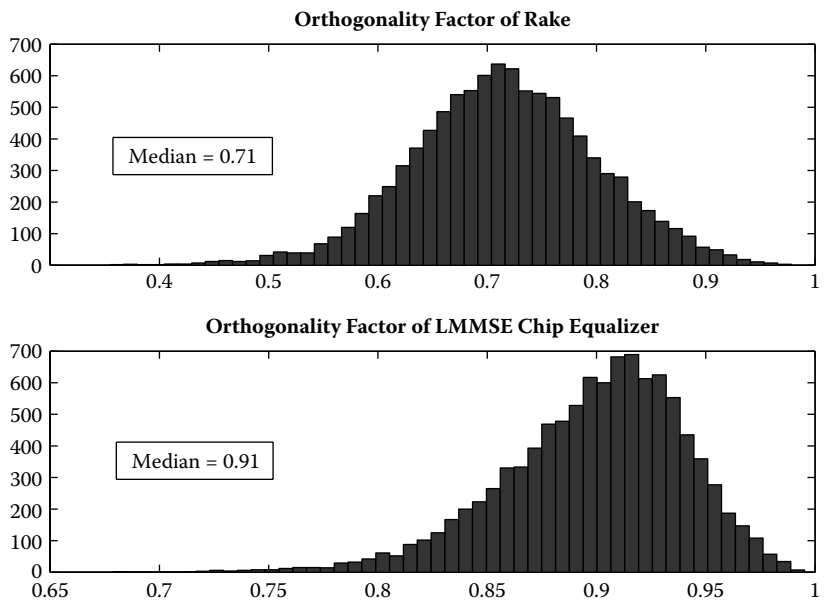

Figure 4.31 Orthogonality factor histograms of two-phase CMF (upper) and two-phase LMMSE chip equalizer (lower) in Vehicular A channel with $\hat{I}_{or}/I_{oc} = 10$ dB.

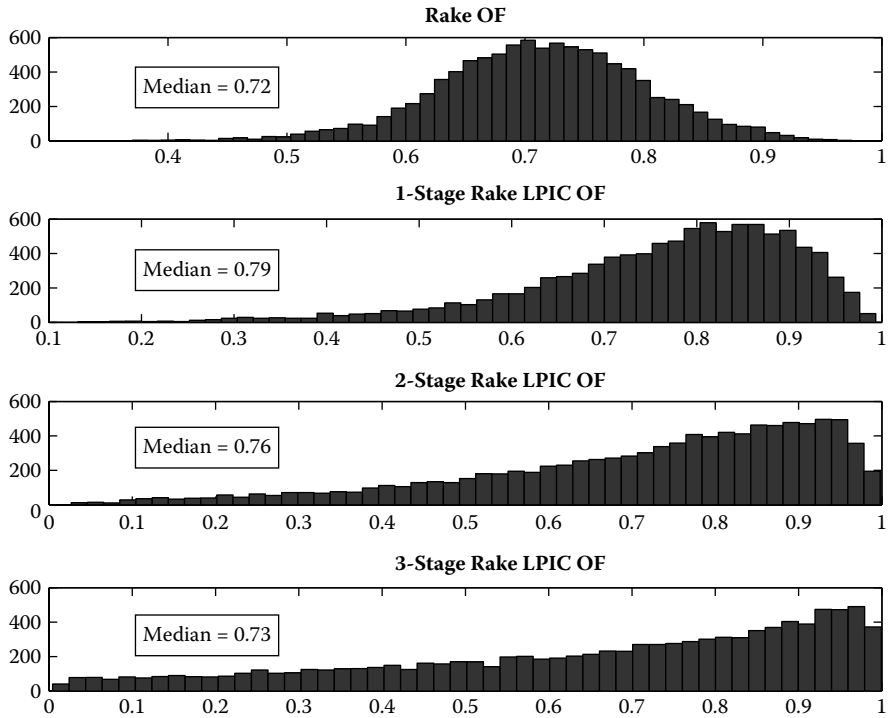

Figure 4.32 Orthogonality factor histogram of conventional LPIC with two-phase CMF in the Vehicular A channel.

Comparing Figure 4.29 and Figure 4.30 we observe that at medium and high $\hat{I}_{or}/I_{oc}$ working regions, hard decisions increase the obtained SINR by 1 to 3 dB. At low $\hat{I}_{or}/I_{oc}$ regions, there is no gain, which is understandable because in those regions hard decisions are not reliable.

We next look at the orthogonality factor (OF) histograms of the considered receivers by randomly generating 10^4 static channels from the Vehicular A power delay profile and an $\hat{I}_{or}/I_{oc}$ value of 10 dB. Figure 4.31 shows the histograms for the CMF and LMMSE equalizer. We see that, besides giving worse median OF, CMF might also give OFs less than 0.4. In Figure 4.32, Figure 4.33 and Figure 4.34 we, respectively, see the trend of OFs obtained from all CMF usage, CMF usage after first stage equalization, and all chip-level LMMSE equalizer usage in LPIC iterations. To obtain these, we first compute the $\|\boldsymbol{\mathcal{X}}_i\|^2$ and pass to OF as $\alpha_i = \frac{1}{1+\|\boldsymbol{\mathcal{X}}_i\|^2}$ since all the filters are unbiased. The histograms in Figure 4.32 clearly demonstrate the problem with conventional LPIC. From a median value perspective, the OF

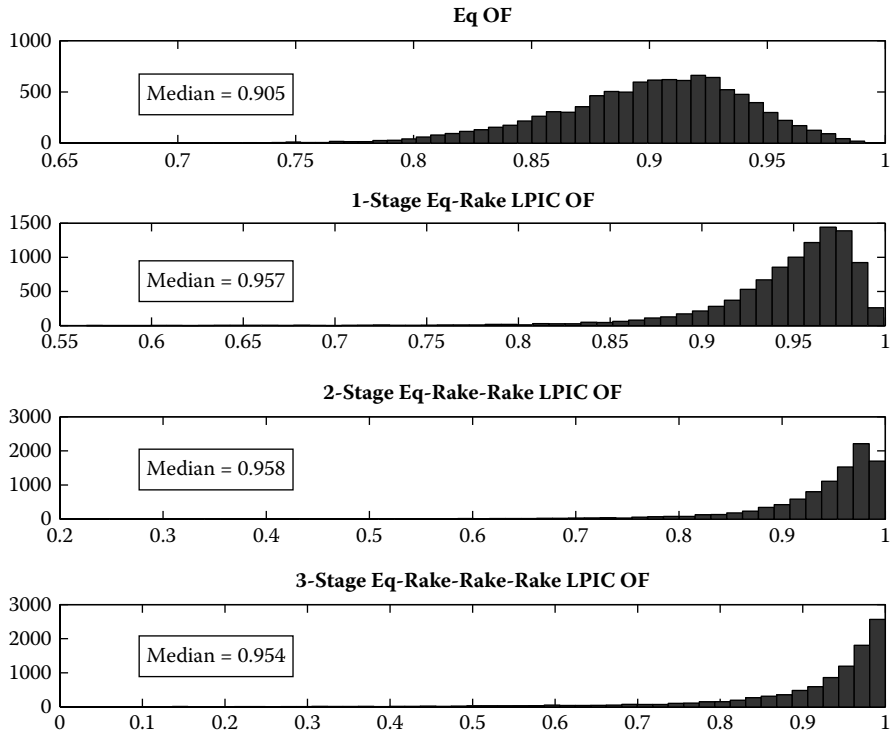

Figure 4.33 Orthogonality factor histogram of LPIC with first stage two-phase LMMSE chip equalizer followed by two-phase CMFs in the Vehicular A channel with $\hat{I}_{or}/I_{oc} = 10$ dB.

first improves at the first stage and then starts degrading. An even more important concern is the widening of the OF range. After four iterations, there are even channel cases where OF is close to zero. The histograms in Figure 4.33 demonstrate the importance of LMMSE chip equalization as a starting point. Although there are still very few corner cases leading to small OFs, the overall performance is at an acceptable level. Finally, the histograms in Figure 4.33 clearly indicate the desirability of using optimized chip equalizers at all stages. Not only the median value but also the worst-case OF improves with each iteration: 0.86 at first and fourth stages, respectively. In brief, we can say that when the mobile knows multiple codes, as in the HSDPA service, applying RAKE receivers after a first-stage equalization stage is a proper choice. In the case of only one code, however, it is beneficial to adapt filters at each stage.

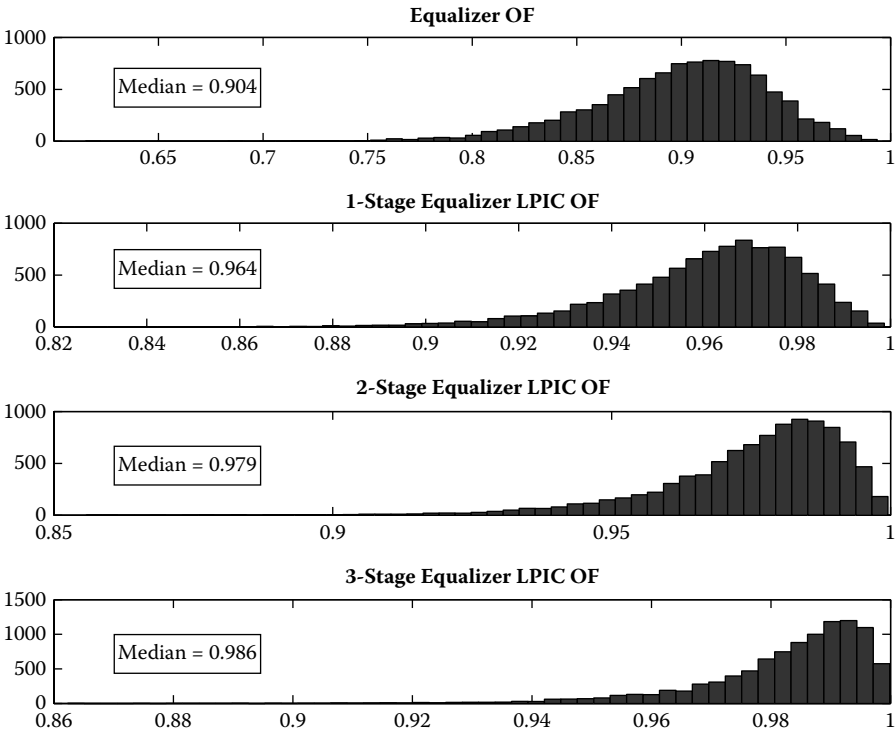

Figure 4.34 Orthogonality factor histogram of LPIC with two-phase LMMSE chip equalizers in all stages in the Vehicular A channel with $\hat{I}_{or}/I_{oc} = 10$ dB.

References

[1] 3GPP. Physical Layer Aspects of HSDPA. Technical Report TS 25.848. [Online]. Available: http://www.3gpp.org/ftp/Specs.

[2] 3GPP. Physical Layer Procedures (FDD). Technical Report TS 25.214. [Online]. Available: http://www.3gpp.org/ftp/Specs.

[3] 3GPP. QoS Concept and Architecture. Technical Report TS 23.107, [Online]. Available: http://www.3gpp.org/ftp/Specs.

[4] 3GPP. Technical Specifications. Technical Report. [Online]. Available: http://www.3gpp.org.

[5] 3GPP. User Equipment (UE) Radio Transmission and Reception (FDD) — Release 8. Technical Report TS 25.101, 3GPP, [Online]. Available: http://www.3gpp.org/ftp/Specs.

[6] 3GPP. UTRA High Speed Downlink Packet Access; Overall UTRAN Description. Technical Report TS25.855. [Online]. Available: http://www.3gpp.org/ftp/Specs.

[7] R.M. Buehrer, S.P. Nicoloso, and S. Gollamudi. Linear versus nonlinear interference cancellation. *J. Commun. Networks*, 1(2): 118–133, June 1999.

[8] C. Cozzo, G.E. Bottomley, and A.S. Khayrallah. Rake receiver finger placement for realistic channels. In *Proc. of the Wireless Communications and Networking Conference*, 2004, pp. 316–321.

[9] H.P. Decell. An application of the Cayley-Hamilton theorem to generalized matrix inversion. *Jr. SIAM Rev.*, 7(4): 526–528, October 1965.

[10] D. Divsalar, M.K. Simon, and D. Raphelli. Improved parallel interference cancellation. *IEEE Trans. Commun. Theory*, 46: 258–268, February 1998.

[11] A. Duel-Hallen. Decorrelating decision-feedback multiuser detector for synchronous code-division multiple-access channel. *IEEE Trans. Commun.*, 41(2): 285–290, February 1993.

[12] P. Frenger, S. Parkvall, and E. Dahlman. The evolution of WCDMA towards higher speed downlink packet data access. In *Proc. Vehicular Technology Conf.,* October 2001.

[13] I. Ghauri and D.T.M. Slock. Linear receivers for the DS-CDMA downlink exploiting orthogonality of spreading sequences. In *Proc. 32nd Asilomar Conf. on Signals, Systems & Computers,* 1: 650–654, November 1998, Pacific Grove, CA.

[14] I. Ghauri and D.T.M. Slock. MMSE-ZF receiver and blind adaptation for multirate CDMA. In *Proc. Vehicular Technology Conf.,* September 1999.

[15] A. Grant and C. Schlegel. Convergence of linear interference cancellation multiuser receivers. *IEEE Trans. Commun.*, 49(10): 1824–1834, October 2001.

[16] L.J. Greenstein, Y.S. Yeh, V. Erceg, and M.V. Clark. A new path gain/delay-spread propagation model for digital cellular channels. *IEEE Trans. Vehicular Technol.*, 46(2): 477–485, May 1997.

[17] H. Holma and A. Toskala. *WCDMA for UMTS*. John Wiley & Sons, 2000.

[18] R. Irmer, A. Nahler, and G. Fettweis. On the impact of soft decision functions on the performance of multistage parallel interference cancelers for CDMA systems. In *Proc. Vehicular Technol. Conf.,* Rhodes, Greece, May 2001.

[19] J.F. Kurose and K.W. Rose. *Computer Networking: A Top Down Approach Featuring the Internet*. Addison-Wesley, 2003.

[20] M. Lenardi and D.T.M. Slock. SINR maximizing equalizer receiver for DS-CDMA. In *Proc. of the EUSIPCO Conf.,* Tampere, Finland, September 2000.

[21] M. Lenardi and D.T.M. Slock. A RAKE structured SINR maximizing mobile receiver for the WCDMA downlink. In *Proc. Asilomar Conf. on Signals, Systems and Computers,* Pacific Grove, CA, November 2001.

[22] R. Lupas and S. Verd'u. Linear multiuser detectors for synchronous code-division multiple-access channels. *IEEE Trans. Information Theory,* IT-35: 123–136, January 1989.

[23] M.F. Madkour, S.C. Gupta, and Y.E. Wang. Successive interference cancellation algorithms for downlink W-CDMA communications. *IEEE Trans. Wireless Commun.,* 1(1): 169–177, January 2002.

[24] U. Madhow and M.L. Honig. MMSE interference suppression for direct-sequence spreadspectrum CDMA. *IEEE Trans. Commun. Theory,* 42: 3178–3188, December 1994.

[25] N.B. Mehta, L.J. Greenstein, T.M. Willis, and Z. Kostic. Analysis and results for the orthogonality factor in WCDMA downlinks. In *Proc. of the Vehicular Technol. Conf.,* May 2002.

[26] S. Moshavi, E. Kanterakis, and D.L. Schilling. Multistage linear receivers for DS-CDMA systems. *Int. J. Wireless Information Networks*, 3(1): 1–17, 1996.

[27] R.R. Muller and S. Verdú. Design and analysis of low complexity interference mitigation on vector channels. *IEEE J. Selected Areas in Commun.*, 19(8): 1429–1441, August 2001.

[28] C. Papadias and D.T.M. Slock. Fractionally spaced equalization of linear polyphase channels and related blind techniques based on multichannel linear prediction. *IEEE Trans. Signal Processing*, 47(3): 641–654, March 1999.

[29] K.I. Pedersen and P.E. Mogensen. The downlink orthogonality factors influence on WCDMA system performance. In *Proc. Vehicular Technology Conf.*, September 2002.

[30] H. Poor and S. Verd'u. Probability of error in MMSE multiuser detection. *IEEE Trans. Information Theory*, 43(3): 858–871, May 1997.

[31] J.G. Proakis. *Digital Communications*, 3rd edition. McGraw-Hill, 1995.

[32] T.S. Rappaport. *Wireless Communications— Principles and Practice*. Prentice Hall, 1996.

[33] L.K. Rasmussen and I.J. Oppermann. Ping-pong effects in linear parallel interference cancellation for CDMA. *IEEE Trans. Wireless Commun.*, 2(2): 357–363, March 2003.

[34] COST Telecom Secretariat, European Commission. COST231 Final Report. Digital Mobile Radio towards Future Generation Systems. Technical report, Brussels, Belgium, 1999.

[35] J.S. Sadowsky, D. Yellin, S. Moshavi, and Y. Perets. Cancellation accuracy in CDMA pilot interference cancellation. In *Proc. Vehicular Technol. Conf.,* April 2003.

[36] J.S. Sadowsky, D. Yellin, S. Moshavi, and Y. Perets. Capacity gains from pilot cancellation in CDMA networks. In *Proc. Wireless Commun. and Networking Conf.,* March 2003.

[37] C. Schlegel, S. Roy, P. Alexander, and Z. Xiang. Multiuser projection receivers. *IEEE J. Selected Areas in Commun.*, 14(8): 1610–1618, October 1996.

[38] D.T.M. Slock and I. Ghauri. A blind maximum SINR receiver for the DS-CDMA forward link. In *Proc. ICASSP'2000,* Istanbul, Turkey, June 2000.

[39] W. Stallings. *Data and Computer Communications, 7th edition*. Prentice Hall, May 2003.

[40] G. Strang. *Introduction to Linear Algebra, 3rd edition*. Wellesley-Cambridge Press, June 1998.

[41] Telecommunication Industry Association. Mobile Station Base-Station Compatibility Standard for Dual-Mode Wideband Spread Spectrum Cellular System. Technical Report TIA/EIA/IS-95, 1993.

[42] D. Tse and P. Viswanath. *Fundamentals of Wireless Communication*. Cambridge University Press, May 2005.

[43] M.K. Varanasi and B. Aazhang. Multistage detection in asynchronous code-division multiple-access communications. *IEEE Trans. Commun. Theory*, 38: 509–519, April 1990.

[44] S. Verdú. *Multiuser Detection*. Cambridge University Press, 1998.

[45] Y.P.E. Wang and G.E. Bottomley. Generalized rake reception for cancelling interference from multiple base stations. In *Proc. Vehicular Tech. Conf.,* Boston, MA, September 2000.

[46] K. Zayana and B. Guisnet. Measurements and modelisation of shadowing crosscorrelations between two base stations. In *Proc. ICUPC,* Rome, Italy, October 1998.

[47] J. Zhang, E.K.P. Chong, and D.N.C. Tse. Output MAI distributions of linear MMSE multiuser receivers in DS-CDMA systems. *IEEE Trans. Information Theory,* 47(3): 1128–1144, March 2001.